

Title page

Copyright 2018

By

Fariba Sadeghinaeenifard

ACKNOWLEDGMENTS

I would like to express my sincere appreciation to my major professor and supervisor Dr. Pinliang Dong, who has helped me a lot in learning programming, selecting the research topic, collecting the data, and developing the research methods. His suggestions and encouragement are crucial for me to enlarge my horizon. I learned a lot from him.

My gratitude also goes to Dr. Xiaohui Yuan and Dr. Chetan Tiwari. They spent a lot of time reading my thesis and providing some useful suggestions.

During the two years of study, many professors have helped me in my research. Dr. Steven Wolverton showed me method-based research design; Dr. Chetan Tiwari, Dr. Waquar Ahmed and Dr. Murray Rice shared many interesting topics in GIS and geography.

Last but not least, I want to thank my parents, my husband Reza Nikfal and my daughter Maneli for their unconditional support and love. Without their support, it is impossible for me to finish my thesis.

TABLE OF CONTENTS

	Page
ACKNOWLEDGMENTS.....	iii
LIST OF TABLES.....	vi
LIST OF FIGURES.....	vii
CHAPTER 1. INTRODUCTION.....	1
1.1 Background.....	1
1.2 Purpose and Significance of the Study.....	3
CHAPTER 2. REVIEW OF LITERATURE.....	5
2.1 Overview.....	5
2.2 3D Shape Descriptors (3D SDs).....	6
2.3 3D Euclidean Distance in Characterizing Individual Tree Crowns.....	9
2.4 The 3D Longitude-Latitude Shape Descriptor for 3D Object Retrieval.....	10
2.5 Image Similarity Assessment Techniques.....	15
2.5.1 Mean Squared Error (MSE).....	16
2.5.2 Peak Signal to Noise Ratio (PSNR).....	16
CHAPTER 3. STUDY AREA AND DATA.....	18
3.1 Study Area.....	18
3.2 Dataset.....	18
CHAPTER 4. METHODOLOGY AND IMPLEMENTATION.....	22
4.1 Definition of Local Coordinate System Relating to Each Tree.....	24
4.2 Learning Salient Point.....	24
4.3 Simulation of LiDAR Point Clouds for the Geometrical Trees.....	26
4.4 Selection of 3D LiDAR Point Clouds for Actual Trees.....	29
4.5 Generation of Reference Shape Signatures from Simulated LiDAR Point Clouds.....	31
4.6 Generation of Evaluated Shape Signatures from Actual LiDAR Point Clouds.....	34
4.7 Similarity Assessment between Evaluated and Reference Shape Signatures.....	43
4.7.1 Subjective Similarity Assessment.....	44
4.7.2 Objective Similarity Assessment.....	45

CHAPTER 5. RESULTS AND DISCUSSION.....	52
CHAPTER 6. CONCLUSION.....	54
REFERENCES.....	58

LIST OF TABLES

	Page
Table 1-1. Comparison of Image and LiDAR-based tree parameters determination.....	2
Table 2-1. Classification of 3D SDs.....	8
Table 3-1 Classes in final point clouds	20
Table 3-2. Tree Species used in this study categorized by their Leaf Trait.....	20
Table 4-1. Flow works of the proposed methodology for shape identification of actual tree	23
Table 4-2. The position and some geometrical properties of all 43 selected trees	30
Table 4-3. Measured times to generate longitude-latitude shape signatures.....	35
Table 4-4. MSEs and PSNRs corresponding to each actual tree and each geometric model, which are used for detecting the most similar shape to each actual tree	46
Table 4-5. Tree canopy can be hemisphere or half-ellipsoid regardless of its leaf trait, which can be identified by its corresponding longitude-latitude shape signature	48

LIST OF FIGURES

	Page
Figure 1-1. Visualization of tree crown formation captured by the artwork of Christo and Jean-Claude.....	2
Figure 2-1. A 3D SD generates the shape signature of its given object, which is compared with SDs of known objects stored in a database for shape retrieval task.....	6
Figure 2-2. Shape Signatures of tree crowns (blue – cone, red – hemisphere, green – half-ellipsoid) resulted from the 3D Euclidian Distance shape descriptor (Dong, 2009).....	10
Figure 2-3. Examples of heads examined for object retrieval by the longitude-latitude shape descriptor (Atmosukarto & Shapiro, 2013)	11
Figure 2-4. Examples of manually marked salient (blue color) and non-salient (red color) points on (a) cat head model, (b) dog head model, and (c) human head model (Atmosukarto & Shapiro, 2008)	12
Figure 2-5. The salient point prediction for (a) cat head, (b) dog head, and (c) human head. The non-salient points are colored in red, while salient points are colored in different shades from green to blue, depending on the classifier confidence score assigned to the point (Atmosukarto & Shapiro, 2008)	13
Figure 2-6. Salient point patterns on 3D objects of Figure 2-5 and their corresponding 2D longitude-latitude map signatures (Atmosukarto & Shapiro, 2008).....	14
Figure 2-7. The objects that are similar and belong to the same class will have similar 2D longitude-latitude signature maps (Atmosukarto & Shapiro, 2008).....	15
Figure 3-1. The location map shows the position of Surrey in British Colombia, Canada	18
Figure 3-2. The footprint of LiDAR coverage over Surrey.....	19
Figure 3-3. LiDAR points on the surface of the deciduous tree and inside it	21
Figure 3-4. LiDAR points collected only on the surface of the evergreen tree	21
Figure 4-1. The left image shows LiDAR point clouds in green and new calculated origin in red color, the table contains converted coordinates of all LiDAR points into that origin named XShifted, YShifted and ZShifted	24
Figure 4-2 Three successive medians divide 3D point clouds into four portions.....	25
Figure 4-3. Points with rank1 are in green color, and points in rank2 are in yellow color	26
Figure 4-4. Interior 3D points generated between two surfaces of the hemisphere	27
Figure 4-5. Hemisphere crown profile	28

Figure 4-6. Half-ellipsoid crown profile	28
Figure 4-7. Interior 3D simulated LiDAR points for the hemisphere and the half-ellipsoid....	29
Figure 4-8. Distribution of all 43 selected trees	30
Figure 4-9. Salient points and their corresponding ranks and colors for the hemispherical and the half-ellipsoidal simulated trees	32
Figure 4-10. Developed ARCGIS toolbox for generation of the shape signature from point clouds.....	33
Figure 4-11. Patterns of salient interior points of hemispherical and the half-ellipsoidal simulated trees and their corresponding map signatures	33
Figure 4-12. The shape signatures generated from surface points and interior points of the hemisphere and the half-ellipsoid	34
Figure 4-13. The profile view of each 43 actual trees, and their corresponding shape signatures.....	43
Figure 4-14. The green part of the hemisphere signature is more widespread than green part of the ellipsoid signature, which is used as a criterion for subjective similarity assessment .	44
Figure 4-15. Developed ArcGIS toolbox named "Mean squared Error" for MSE similarity assessment.....	46
Figure 4-16. θ and ϕ of a single 3D point P	49
Figure 4-17. Two points P and P' aligned with the local origin have the same normal vector n, and the same longitude and latitude.....	49
Figure 4-18. Visual comparison of shape signatures or 3D profile views approve objective similarity assessment result for evergreen1.....	50
Figure 4-19. Visual comparison of shape signatures or 3D profile views approve objective similarity assessment result for deciduous3	51
Figure 4-20. Visual comparison is not able to identify the exact shape of tree canopy for evergreen9, so that we can rely on objective similarity assessment result.....	51

CHAPTER 1

INTRODUCTION

1.1 Background

Tree crown characterization is essential for the variety of forest-related activities, such as natural resource management, silviculture treatments, monitoring activities, biomass estimation, biodiversity monitoring, wildlife habitat assessment, and wildfire risk assessment. It can also be used to improve vegetation/ecosystem modeling (Lichstein, 2010).

There are several ways for gathering data on forest ecosystems, including situ (field) measurements, high spatial resolution imagery, and Light Detection and Ranging (LiDAR). Jakubowski et al. (2013) have summarized past studies to detect and delineate individual trees from imagery, LiDAR, and their combination.

For individual trees in small study areas, field measurement is an excellent option to capture information on tree parameters at low cost (Sexon, Bax, Siqueira, Swenson, & Hensley, 2009). However, in situ data collection is time consuming and costly over large areas and remote regions. Conversely, remote sensing provides the best alternative approach to derive information (Ghosha, Fassnacht, Joshi, & Koch, 2014). Light Detection and Ranging (LiDAR), as a relatively new technology, has been established as a promising way for broad-scale mapping and modeling individual tree parameters in three dimensions (3D), because laser beams could penetrate through the foliage and collect point clouds with highly accurate 3D coordinates (Xiao, 2012).

Table 1-1 indicates different types of possible biophysical parameters extracted from optical imagery and LiDAR data alone. According to Table 1-1, it infers that optical imagery allows us to detect at most 2D dimensional biophysical parameters, while LiDAR data provides a way to determine 3D dimensions of tree parameters.

Table 1-1. Comparison of Image and LiDAR-based tree parameters determination

		Image-based	LiDAR-based
Tree detection	✘	✓	✓
Tree delineation	👉	✓	✓
3D delineation	📦		✓

More recently, LiDAR technology has improved and expanded to yield a higher density of points (over 25 points per square meter), so it has become increasingly possible to successfully detect and delineate individual trees and precisely measure their metrics, such as tree crown parameters (Jakubowski , Li, Guo, & Kelly, 2013). Some parameters, such as canopy closure and tree height, can be directly measured using LiDAR data alone, while some other parameters, such as biomass and diameter at breast height, can be modeled using LiDAR and field data. However, discrimination of different tree crowns, based on their 3D shapes, remains a significant challenge.

Tree crown complexity attracts artists’ attention as well, as Christo and Jeanne Claude visualized this complexity by wrapping up real trees with fabric, as shown in Figure 1-1 (Kato, et al., 2009).



Figure 1-1. Visualization of tree crown formation captured by the artwork of Christo and Jean-Claude

1.2 Purpose and Significance of the Study

Previous researchers have focused on tree height, crown width, basal area, crown base height, and crown volume using LiDAR data. There are few studies focused on automated characterization of 3D canopy shapes using LiDAR data (Omasa & Fumiki, 2007; Dong, 2009; Liu, 2013; Kato, et al., 2009).

The shape and size of tree crowns are related to photosynthesis, nutrient cycling, energy transfer (evaporation and respiration) and light transmittance to beneath vegetation (Kato, et al., 2009). Due to the irregularity of crown shapes of trees, obtaining precise crown shape information becomes a challenging task, and is difficult to capture using traditional-forest equipment.

Implicit surface reconstruction has been widely used in field of computer graphics to construct 3D models of physical objects from noisy scanned laser points (Kato, et al., 2009).

Although, there are numerous proposed shape measures in fields of computer vision, graphics, pattern recognition, and machine intelligence in the last decades, the application of these measures in other areas such as geography, forestry, and ecology has been relatively limited (Dong, 2009).

Ever-growing 3D shape descriptors within the computer science field, along with their strengths and weaknesses, have provided an open research area for evaluation of newly introduced 3D shape descriptors aimed at tree crown discrimination. Apparently, a few researchers are focusing in this context and there is a broad gap that requires more attention.

Therefore, the primary objective of the study is to develop a modified 3D shape descriptor for discrimination of different tree crown shapes using LiDAR point clouds. This study will address the following research questions:

- (1) Which existing 3D shape descriptor is recommended in computer graphics for 3D object retrieval?
- (2) How should a successful 3D shape descriptor in computer graphics modify for effective tree crown shape discrimination applied on LiDAR data?
- (3) Can simulated LiDAR point clouds for geometrical-shaped trees be used as references to reveal the shape of real LiDAR point clouds of actual trees?
- (4) How can we automatically discriminate three-dimensional tree crown shapes using LiDAR data?

CHAPTER 2

REVIEW OF LITERATURE

2.1 Overview

By the rapid growing of 3D objects in the virtual world including computer games, movies, TV and engineering design, medical diagnostic, architectural and cultural heritage, 3D object retrieval techniques have turned into a hot topic among computer science researchers. One of the essential applications of 3D object retrieval is retrieving 3D models and images on the internet. Currently, the conventional way to search images and 3D models over the internet is via text and queries. Retrieval of images, using another image as a query (the result of a 3D shape descriptor), is still not sophisticated enough to provide us with the desired results (Khalid Kazmi, You, & Zhang, 2013). Classification and retrieval techniques for text, images, and videos cannot be directly applied to 3D objects, because 3D objects have different data characteristics from other data modalities (Atmosukarto & Shapiro, 2013).

Due to its importance, researchers in the area of computer science have taken the initiative to organize an annual 3D shape retrieval evaluation called the 3D Shape Retrieval Contest (SHREC) that started in 2006. The general objective is to evaluate the effectiveness of 3D shape retrieval algorithms based on a benchmark (Atmosukarto & Shapiro, 2008; Khalid Kazmi, You, & Zhang, 2013). Thus, this study has been designed to validate one of these existing 3D shape retrieval algorithms in the field of geography.

This chapter contains the following sections. The author first discusses Shape Descriptor (SD) definition, essential characteristics of an effective SD, and classification of different 3D SDs. Next, I explain the only research (until 2018), applied a 3D SD on LiDAR point clouds aimed at tree crown discrimination. I then describe a study conducted in the computer science field to retrieve 3D objects using a 3D shape descriptor, known as a longitude-latitude

transformation, which performs on different object heads. This approach motivated me to validate its efficiency in the geography field, mainly for tree crown differentiation applied on LiDAR point clouds. Since, the result of the longitude-latitude transformation is a 2D spatial map; and comparison of 2D maps requires image similarity assessment techniques, therefore, I discuss two of the simplest and the most useful similarity assessment techniques proposed in the computer science field.

2.2 3D Shape Descriptors (3D SDs)

A 3D shape descriptor is a mathematical function that is applied to an object and produce numerical values, which are representative of a particular characteristic of the object (Martinez-Ortiz, 2010). The nature and meaning of such values depend on the definition of the shape descriptor. These numerical values are called signatures, and introduced as input features to a classifier to determine the class membership of its given object. In other words, extracted shape signature can be considered as a query, and compared with numerical values of all known objects, which already stored in the database, to retrieve the database object, which has similar numerical values to the query. Figure 2-1 shows a graphical view of definition of a 3D Shape Descriptor.

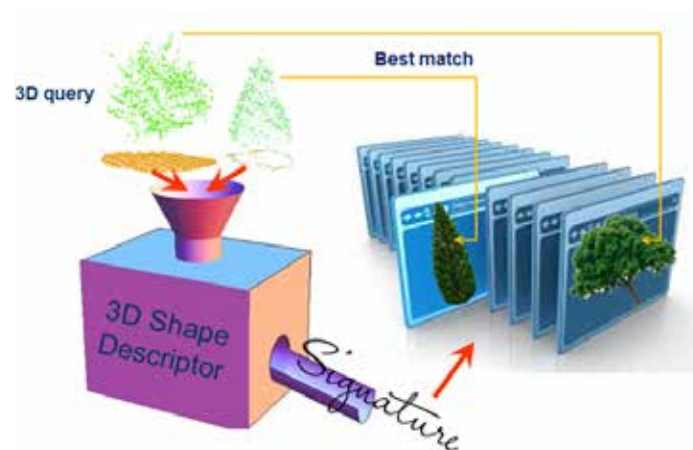


Figure 2-1. A 3D SD generates the shape signature of its given object, which is compared with SDs of known objects stored in a database for shape retrieval task

SDs are evaluated based on some characteristics that define the overall quality and effectiveness of a shape descriptor (Khalid Kazmi, You, & Zhang, 2013), although they are not strictly speaking requirements for all shape descriptors (Martinez-Ortiz, 2010). The following is a list of some of these desirable properties of a successful SD: (Iyer, Jayanti, Lou, Kalyanaraman, & Ramani, 2005; Yang, Kpalma, & Ronsin, 2008; Martinez-Ortiz, 2010)

- a) Uniqueness: each unique shape has its own unique shape signature.
- b) Discriminative accuracy: the objects found perceptually similar by human have the same shape signatures, and different from others.
- c) Well-defined range: having an idea of the range of values produced by a shape descriptor is very important for interpreting the meaning of the values provided by the descriptor. Also, it might be useful to know the range generated by a descriptor for designing an application (in case normalization is required).
- d) Transformation (translation, scaling, and rotation) invariance. The location, rotation, and scaling changing of the shape must not affect the extracted shape signature.
- e) Insensitive to noise: the shape descriptor must be as robust as possible against noise, i.e., small changes in the shape lead to small changes in its corresponding signature.
- f) The shape descriptor should be efficient, regarding computational performance and memory.

Apparently, no single descriptor performs the best for all kinds of retrieval tasks. Each descriptor had its strength and weakness across retrieval tasks. Researchers in 3D search engines have widely used 3d SDs, which are classified into five broad categories and their related subcategories, as shown in Table 2-1. Among various 3D SDs, the graph-based are the least favored algorithms due to their inefficient performance. In contrast, the view-based and histogram-based algorithms are the most favored SDs, because of their fundamental decency and performance (Khalid Kazmi, You, & Zhang, 2013).

Table 2-1. Classification of 3D SDs

View-Based	Adaptive Views Clustering Compact Multi-View Descriptor Light Field Descriptor(LFD)
Histogram-Based	Shape Spectrum Generalized shape distributions Bag-of-Features
Transform-Based	Spherical Harmonics Descriptor PCA Spherical Harmonics Trans. Spherical Trace Transform
Graph-Based	Skeletal Graph-Based Reeb Graph-Based
Hybrid 3D Descriptors	CMVD + STT Depth-Buffer+Silhouette+REXT SIFT + Bag of Features Depth-Buffer + Spherical Harmonics

To benefit from the advantages of the histogram-based SDs, in this study a histogram-based SD is used that falls explicitly into the shape spectrum subcategory. So, only this category is discussed in extent detail, and information about other groups can be found in (Khalid Kazmi, You, & Zhang, 2013; Martinez-Ortiz, 2010).

Histogram-based descriptors collect the features of a 3D shape in numerical values in bins defined over the feature domain. A 3D Shape Spectrum Descriptor (3D SSD) is a shape descriptor, which contains a shape index distributed over the entire mesh (Zaharia & Preteux, January 2001). A shape index is a local geometric feature of the shape expressed as the angular coordinate of the polar representation of the principal vector. Regarding the original feature, the shape index is invariant to scale and Euclidean transform, and it represents by salient elementary shapes (Khalid Kazmi, You, & Zhang, 2013). The accuracy of a shape-based

retrieval system largely depends on finding a suitable descriptor, which can represent the local and global characteristics of a 3D object, by encapsulating the critical shape properties of the object. This process is not a trivial task (Atmosukarto & Shapiro, 2008).

In general, previous studies have indicated the effectiveness of 3D shape descriptors in object retrieval in computer graphics (Osada, Funkhouser, Chazelle, & Dobkin, 2002; Atmosukarto & Shapiro, 2013). In particular, few researchers have focused on the application of 3D shape descriptors in the field of geography, which is of interest to this study.

2.3 3D Euclidean Distance in Characterizing Individual Tree Crowns

Dong (2010), in the area of geography, has demonstrated successful results in characterizing individual tree crowns using shape signatures applied on simulated point clouds and manually selected samples of LiDAR for oak and Douglas fir crowns in both vector and raster formats.

Dong (2010) used Euclidean distance, as a 3D shape descriptor, to detect differentiation between various tree canopy shapes. The author calculated Euclidean distance between any two random points, either simulated random points or actual LiDAR point clouds. After a certain number of iteration (e.g., 10,000) of the distance calculation, 50 histogram bins were used to summarize the frequency distribution of the distances between point-pairs, which then converted to a probability distribution for comparison between different 3D crown shapes. Figure 2-2 demonstrates the 3D Shape signatures resulting from trees with three geometric models, including cone, hemisphere, and half-ellipsoid.

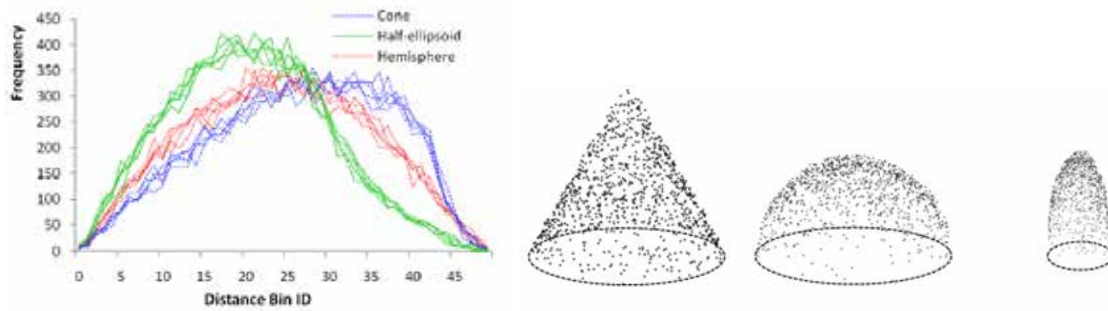


Figure 2-2. Shape Signatures of tree crowns (blue – cone, red – hemisphere, green – half-ellipsoid) resulted from the 3D Euclidian Distance shape descriptor (Dong, 2009)

Then, the correlation coefficients were calculated as measures of similarity between 3D shape signatures. The results from different runs of the same crown model have shown high correlation coefficients of over 0.99, whereas the lower correlation coefficients were obtained, when comparing two different 3D crown shape signatures. The obtained results indicated that the shape signatures are similar within the same group of trees, while different between different groups of trees. Lastly, Dong (2010) concluded that comparison of 3D crown shapes may be effectively reduced to the comparison of frequency distributions of distances between random points.

2.4 The 3D Longitude-Latitude Shape Descriptor for 3D Object Retrieval

Atmosukarto and Shapiro (2008), in the field of computer science, contributed the longitude-latitude transformation as a shape-based descriptor, to retrieve 3D objects. They examined heads of different objects, including cat head, dog head, human head, rabbit head, horse head, tiger head and bear head to test the performance and repeatability of their proposed methodology on general 3D object classification, where objects in the dataset are not very similar. Figure 2-3 shows examples of the head objects of the seven classes.



Figure 2-3. Examples of heads examined for object retrieval by the longitude-latitude shape descriptor (Atmosukarto & Shapiro, 2013)

The digitized 3D objects were obtained by scanning hand-made clay toys using a laser scanner. In order to increase the number of 3D objects for training, the authors used 3D Studio Max software and created new objects by deforming the original scanned 3D models in a controlled fashion. Then, the raw data from the scanner, which consists of 3D point clouds, were further processed to obtain smooth and uniformly sampled meshes of 0.9-1.0 mm resolution. In other words, a surface mesh representing a 3D object consists of points $\{p_i\}$ on the object surface and information about the connectivity of all points.

Afterward, the authors used a learning approach to identify interesting local features or salient points on the 3D object, by applying a low-level operator to every point on the surface mesh. The low-level operators extract local properties of the surface points by computing a single feature value u_i for every point p_i on the mesh surface.

The base framework of their methodology executes two phases, the low-level feature extraction, and the mid-level feature aggregation. The low-level feature value u_i constitutes of Gaussian curvature, Besl-Jain surface curvature characterization and azimuth-elevation angles of the surface normal vector. Detailed information about the low-level feature calculation can be found in Atmosukarto and Shapiro (2013). Afterward, the low-level feature values are convolved with Gaussian filter to reduce noise.

After the first step, every point p_i on the surface mesh will have the low-level feature value u_i . The second step performs the mid-level feature aggregation to compute a number of values for a given neighborhood of every point p_i on the surface mesh. In this work, the

authors used a local histogram to aggregate the low-level feature values of each point. The histograms are computed by taking a neighborhood around each point and accumulating the low-level features in that neighborhood. The feature aggregation results of the base framework are used to determine salient points of an object using a learning approach.

The authors used a learning approach to find salient points on a 3D object. In this approach, an expert marks training points on the 3D objects for a particular application. The marked salient points on 3D head models are anatomical landmarks of the face and included the tip of the nose, corners of eyes, and both corners and midpoints of lips, etc. as shown in Figure 2-4.

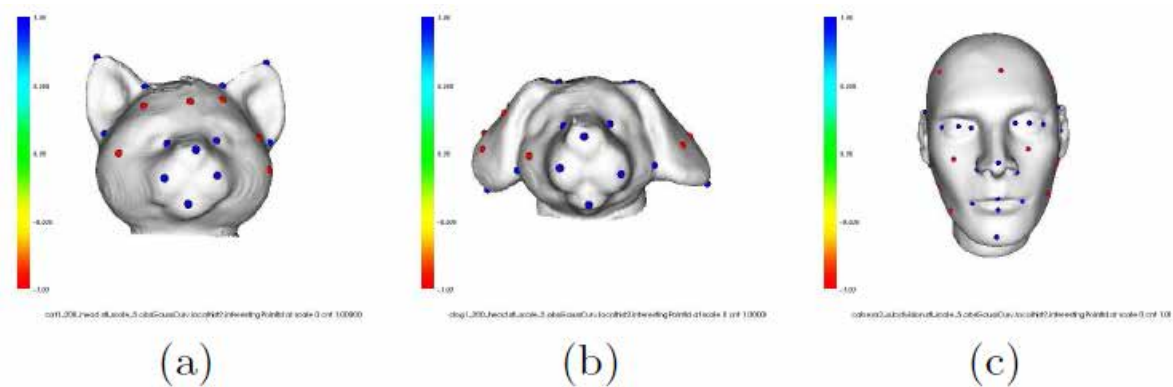


Figure 2-4. Examples of manually marked salient (blue color) and non-salient (red color) points on (a) cat head model, (b) dog head model, and (c) human head model (Atmosukarto & Shapiro, 2008)

After training, a classification was required to detect salient points based on their characteristics. So, the authors developed a salient point classifier that identifies points that have a combination of high curvature and low entropy values. The salient point histograms have low bin counts in the bins corresponding to low curvature values and a high bin counts in the highest curvature bin. While, the non-salient point histograms have medium to high bin counts in the low-curvature bins. Therefore, histograms of low-level feature values obtained in the base framework are used to train a support vector machine (SVM) classifier to learn the salient points on the 3D surface mesh. Therefore, the classifier labels each points of any

3D object as either salient or non-salient, and provides a confidence score for its decision. A threshold is applied to keep only salient points with high confidence scores (≥ 0.95). While, the classifier was only trained on cat heads, dog heads, and human heads (Figure 2-5), it did a good job of finding salient points in the other classes. The salient points are colored according to the assigned classifier confidence score. The non-salient points are colored in red, while salient points are colored in different shades, ranging from green to blue, depending on the classifier confidence score assigned to the point. A threshold ($T = 0.95$) was applied to include only salient points with high confidence scores.

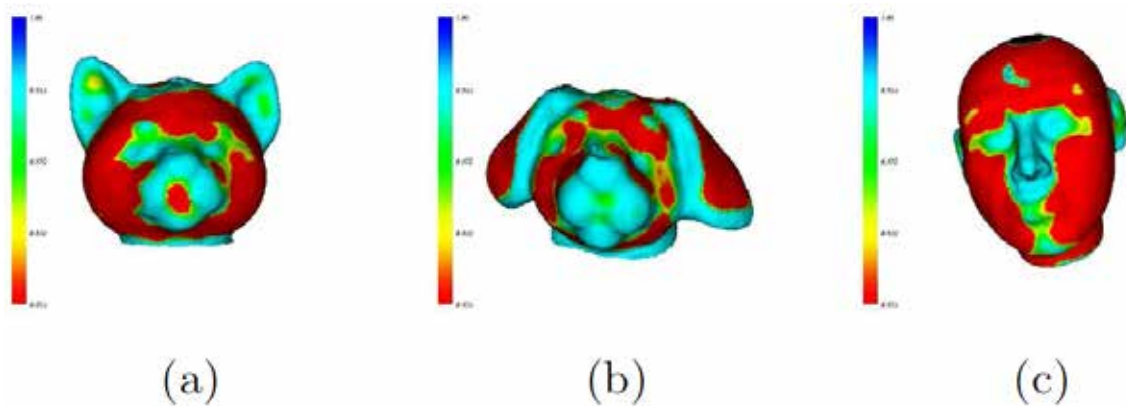


Figure 2-5. The salient point prediction for (a) cat head, (b) dog head, and (c) human head. The non-salient points are colored in red, while salient points are colored in different shades from green to blue, depending on the classifier confidence score assigned to the point (Atmosukarto & Shapiro, 2008)

Then, the authors introduced a 3D shape descriptor called a longitude-latitude SD for describing shape and properties of any 3D objects to classify them. Therefore, the shape signature of a 3D object is obtained based on the salient point patterns of the object mapped onto a 2D plane via the longitude-latitude transformation.

Before mapping the salient point patterns onto the 2D longitude- latitude plane, the salient points were assigned a label according to their classifier confidence score. The classifier confidence score range is discretized into a number of bins. In this experiment, the authors discretized the confidence score range from 0.95 and above into five bins. Hence,

each salient point on the 3D mesh is assigned a label based on the bin into which its confidence score falls.

Then, the longitude and latitude positions of all 3D points on the object's surface were calculated. Given any point $p_i (p_{ix}, p_{iy}, p_{iz})$, the longitude position θ_i and the latitude position ϕ_i of point p_i are calculated as follows:

$$\theta_i = \arctan \left(\frac{p_{iz}}{p_{ix}} \right) \quad \phi_i = \arctan \left(\frac{p_{iy}}{\sqrt{(p_{ix}^2 + p_{iz}^2)}} \right) \quad \text{Equation 2-1}$$

$$\text{Where } \theta_i = \left[-\frac{\pi}{2}, \frac{\pi}{2} \right] \text{ and } \phi_i = \left[-\frac{\pi}{2}, \frac{\pi}{2} \right]$$

The signature map of the longitude and latitude positions of all 3D points on the object is created by binning the longitude and latitude values of points into a fixed number of bins. A bin is labeled with the salient point label which falls into that bin (Atmosukarto & Shapiro, 2008).

Atmosukarto and Shapiro (2008) demonstrated salient point patterns for the cat head, dog head, and human head and their corresponding 2D longitude-latitude map signatures as shown in Figure 2-6.

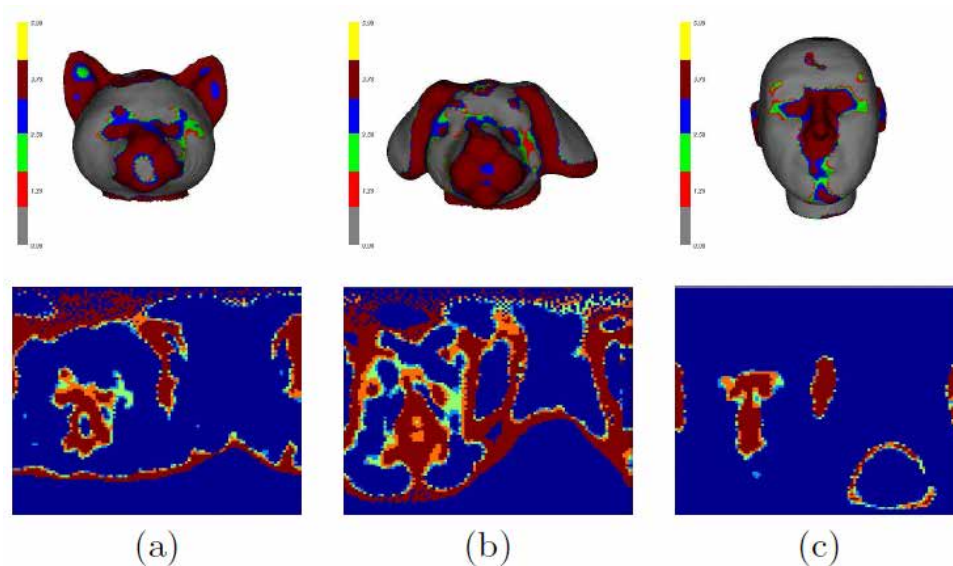


Figure 2-6. Salient point patterns on 3D objects of Figure 2-5 and their corresponding 2D longitude-latitude map signatures (Atmosukarto & Shapiro, 2008)

Furthermore, Figure 2-7 illustrates how different objects belonging to the same class have similar longitude-latitude signature maps.

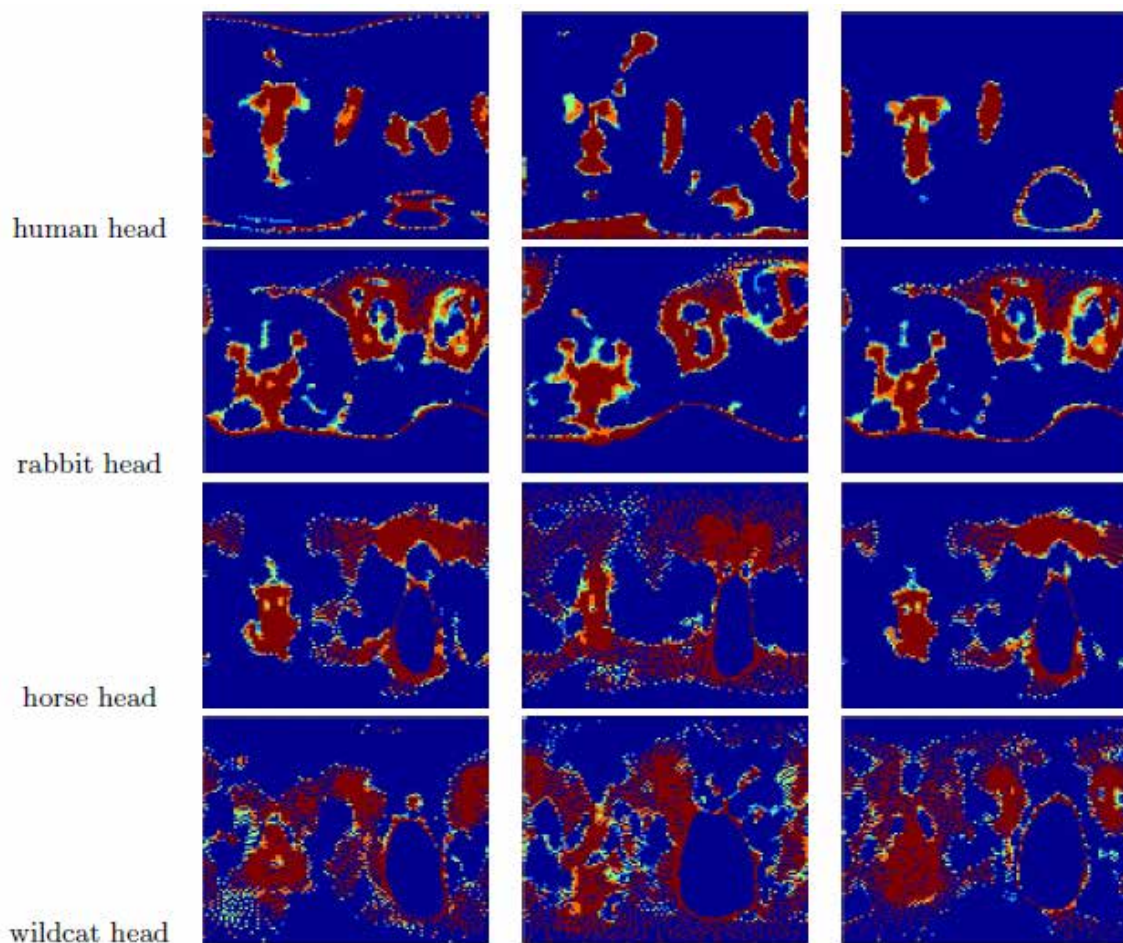


Figure 2-7. The objects that are similar and belong to the same class will have similar 2D longitude-latitude signature maps (Atmosukarto & Shapiro, 2008)

Retrieval task of 3D objects is then performed by calculating the distance between the query object signature and all signatures in the database. Then, the retrieval algorithm returned the object, which has a signature similar to the 2D signature map of the query. Eventually, Atmosukarto and Shapiro (2008) concluded that the 2D longitude-latitude map signature achieved a good retrieval score for 3D object recognition.

2.5 Image Similarity Assessment Techniques

Measurement of image similarity is crucial for many image processing applications.

There are basically two approaches for image similarity assessment, objective and subjective (Varnan, Jagan, Kaur, Jyoti, & Rao, September 2011). In subjective approaches, some observers are selected, tested for their visual capabilities, shown a reference image and a series of evaluated images and asked to score the similarity of the images being assessed. It is the only “correct” method of similarity assessment. However, subjective evaluation is usually inconvenient, time-consuming and expensive. In contrary, these are various automatic algorithms for similarity assessment known as objective approaches that could analyze images and report their similarity scores without human involvement. Such methods could eliminate the need for expensive subjective studies (Varnan, Jagan, Kaur, Jyoti, & Rao, September 2011). The similarity of an image could be assessed by comparing it against a reference image by using simple statistic error metrics. There are large varieties of such metrics, which only two of existing measures discussed below.

2.5.1 Mean Squared Error (MSE)

One obvious way to measure the similarity is computing the error signal by subtracting the test signal from the reference, and then computing the average energy of the error signal.

The Mean Squared Error (MSE) is defined as follows:

$$MSE = \frac{1}{MN} \sum_{i=1}^M \sum_{j=1}^N (x(i, j) - y(i, j))^2 \text{ Equation 2-2}$$

where $x(i, j)$ represents the reference image and $y(i, j)$ represents the evaluated image and i and j are the pixel position of any $M \times N$ image.

2.5.2 Peak Signal to Noise Ratio (PSNR)

The PSNR is evaluated in decibels and is inversely proportional the Mean Squared Error. Following equation gives PSNR:

$$PSNR = 10 \log_{10} \frac{(2^n - 1)^2}{MSE} \quad \text{Equation 2-3}$$

The simplest and the most widely used similarity assessment measures are MSE and PSNR. These are appealing, because they are simple to calculate, have obvious physical meaning and mathematically easy to implement (Varnan, Jagan, Kaur, Jyoti, & Rao, September 2011). With PSNR, greater values indicate greater image similarity, while with MSE greater values indicate lower image similarity.

CHAPTER 3

STUDY AREA AND DATA

3.1 Study Area

The research area is the city of Surrey located in the Greater Vancouver regional district, province of British Columbia, Canada between $49^{\circ} 0' 58.89''$, $122^{\circ} 54' 43.51''$ and $49^{\circ} 13' 1.06''$, $122^{\circ} 40' 2.88''$ (Figure 3-1). Over 90,000 trees are actively managed on its property, and 3500-5000 trees are being planted annually. The city spends roughly 600,000 USD to water trees every year as part of its tree maintenance plan (Plowright, Coops, Eskelson, Sheppard, & Aven, 2016).



Figure 3-1. The location map shows the position of Surrey in British Columbia, Canada

The city of Surrey maintains a comprehensive GIS database of all trees that it plants and manages. Each entity includes a tree species, subspecies, planting date and approximate geographic coordinates.

3.2 Dataset

Airborne LiDAR data was acquired over Surrey by Airborne Imaging (Calgary, Alberta),

under contract with the city in April 2013. The footprint of the LiDAR coverage is shown in Figure 3-2.



Figure 3-2. The footprint of LiDAR coverage over Surrey

The entire point clouds were produced in UTM zone 10 and NAD1983 datum. The assessment of the vertical accuracy of the point clouds on flat surfaces in 95% confidence interval is less than 9 centimeters, and estimated of horizontal accuracy for this data set is better than 15 cm in 95% of the time (Airborne Imaging, 2013).

A Leica ALS70-HP discrete return LiDAR system, with up to four discrete returns per pulse, was flown at 1000 m above ground level with 688 m swaths with 50% overlap. The pulse rate was 500 KHz, which resulted in an average first-return density of 25 points per square meter. Before being delivered by the contractor, the raw LiDAR point clouds were classified into land class covers, such as ground, building or vegetation, using TerraScan software as shown in Table 3-1 (TerraSolid Ltd., Helsinki). A 1 m² rasterized digital elevation model (DEM) interpolated from classified ground points using a triangular irregular network (TIN) was also supplied.

Table 3-1 Classes in final point clouds

Class ID	Class	Description
2	Ground	
3	Low Vegetation (0 to 0.7m)	
4	Medium Vegetation (0.7to 2m)	
5	High Vegetation (above 2m)	
6	Buildings (and Bridges)	
7	Low Points (noise)	Manually Identified
9	Water	
11	Withheld	Automatically Identified

Since trees captured under leaf-off conditions, I have grouped them by their characteristic including leaf structures and leaf traits (deciduous or evergreen), and illustrated in Table 3-2. Since LiDAR point clouds and GIS data of the Surrey were precisely geo-referenced, any field data collection for geo-referencing is not required.

Table 3-2. Tree Species used in this study categorized by their Leaf Trait

Genera	Leaf structure	Leaf trait	
		Evergreen	Deciduous
Picea	Clustered needles	✓	
Pseudotsuga	Flat, single needles	✓	
Tsuga	Flat, single needles	✓	
Sequoia	Flat, single needles	✓	
Thuja	Scale-like leaves	✓	
Acer	Opposite, simple leaves		✓
Sorbus	Alternate, compound leaves		✓
Prunus	Alternate, simple leaves		✓
Malus	Alternate, simple leaves		✓
Quercus	Spirally arranged, lobed leaves		✓
Betula	Simple leaves, toothed or pointed		✓
Ulmus	Alternate, simple single or doubly serrated leaves		✓
Magnolia	Simple, smooth-edged leaves		✓

Note that, deciduous trees were not developing leaves when the LiDAR data was acquired, which could influence on the type of LiDAR points collected over tree canopy, since Laser beams pass through the tree canopy. In other words, for a single deciduous tree taller than 2 meters, collected LiDAR points show a different range of classes such as medium, low and high vegetation and even ground. Conversely, permanent leaf formation of evergreen trees does not allow laser beams pass within the canopy, so collected points fall into a class related to the surface of the canopy. Figure 3-3 shows captured LiDAR points on the surface of the deciduous tree and inside it, due to penetration of laser beam through the leaf-off canopy and reaching the ground, while Figure 3-4 indicates LiDAR points collected only on the surface of the evergreen tree, because laser beams become blocked by leaves.

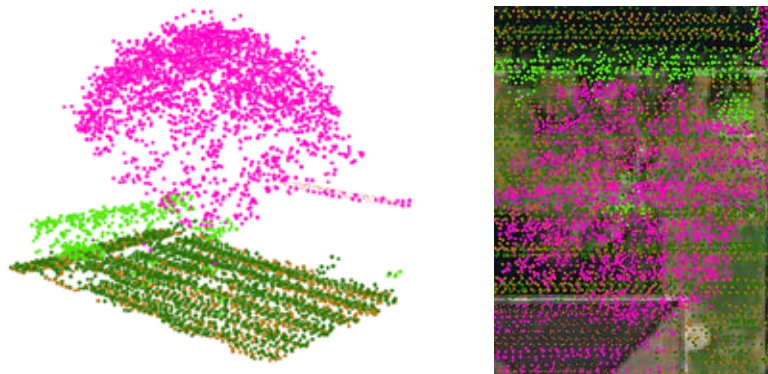


Figure 3-3. LiDAR points on the surface of the deciduous tree and inside it

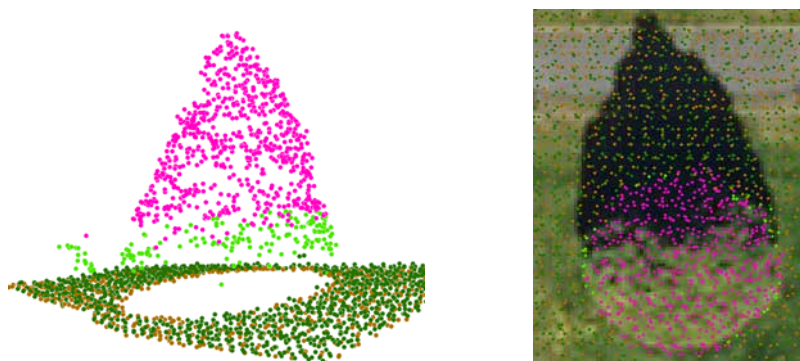


Figure 3-4. LiDAR points collected only on the surface of the evergreen tree

CHAPTER 4

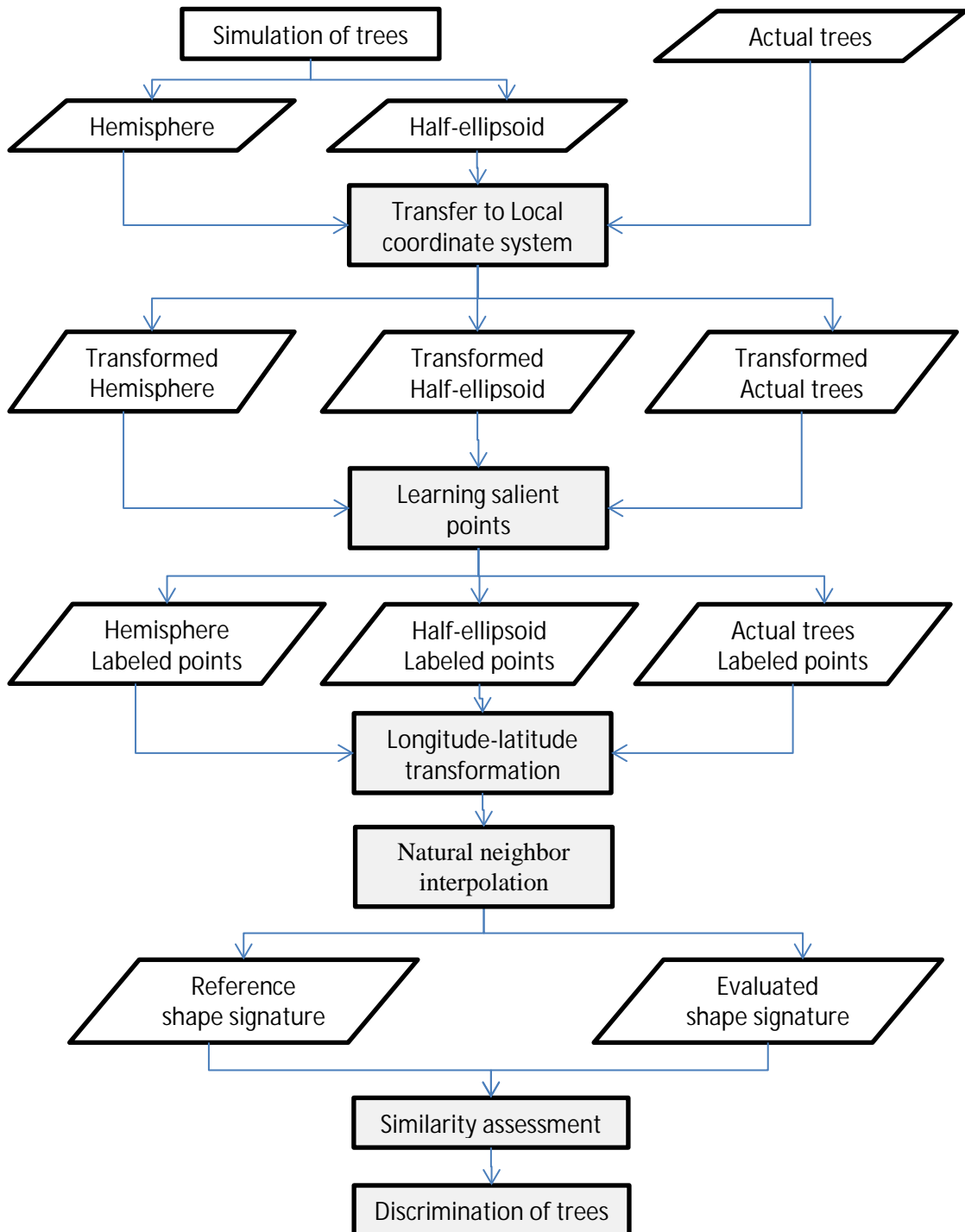
METHODOLOGY AND IMPLEMENTATION

This study is designed to examine the effectiveness and capability of the longitude-latitude shape descriptor for tree crown discrimination. The proposed method involves only LiDAR point clouds of individual trees with different geometric shapes, either evergreen or deciduous, and does not handle trees represented by Canopy Height Model (CHM), due to the limited number of pixels.

The proposed methodology comprises of five main components (refer to Table 4-1), including the definition of a local coordinate system, learning salient points, generation of simulated LiDAR point clouds with geometrical shape, shape signature generation from simulated LiDAR points and actual LiDAR point clouds, and finally similarity assessment of shape signatures. The first component represents a proposed strategy to define a local coordinate system relating to each tree to normalize 3D point clouds. The second component explains a proposed learning approach to categorize all 3D point clouds to identify interesting or salient points on each tree. The third component discusses generating simulated LiDAR point clouds for two geometrical trees, including a hemisphere and a half-ellipsoid. Then, actual LiDAR point clouds captured on either evergreen or deciduous trees are used for introducing to the next component. The fourth component explains how the longitude-latitude shape descriptor is involved in the experiment for generating shape signatures from point clouds, either on the simulated or actual tree. At this step, shape signatures are in point format. In order to make feasible any further comparison, natural neighbor interpolation based on assigned rank is applied to the point map to generate raster format of the shape signature. The generated shape signatures from simulated and actual LiDAR points are called reference and evaluated shape signatures, respectively. Finally, the fifth component

determines the similarity between evaluated and reference shape signatures to discriminate experimented trees based on their shape.

Table 4-1. Flow works of the proposed methodology for shape identification of actual tree



4.1 Definition of Local Coordinate System Relating to Each Tree

All 3D points of trees, either on the simulated or actual trees, are transformed to a local coordinate system by definition of a new origin. The new origin is defined inside each tree by calculating the median value of x, y and z positions of all 3D points on each tree either simulated or actual point clouds. Then the x, y, z coordinates of 3D point clouds are transformed to this new origin. As a result, the actual LiDAR point clouds with 6 and 7 digits for the x and y positions and 3 digits for the z position in the UTM coordinate system are converted into only one digit; likewise, the simulated LiDAR point clouds which are in the unknown coordinate system and mostly with one digit for x, y and z positions. Figure 4-1 shows a collection of LiDAR points, calculated new origin and converted coordinates to the new coordinate system.

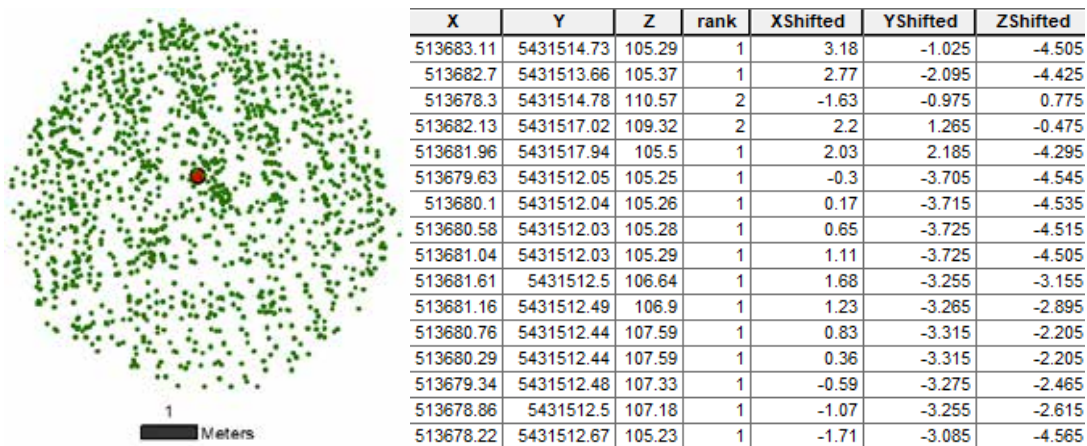


Figure 4-1. The left image shows LiDAR point clouds in green and new calculated origin in red color, the table contains converted coordinates of all LiDAR points into that origin named XShifted, YShifted and ZShifted

4.2 Learning Salient Point

The purpose of the learning salient point is finding the characteristics of salient points of 3D point clouds related to each tree, and then the transformed pattern of the salient points to a signature map is used for further analysis. In this study, a new methodology for learning salient points is proposed. This method differs from the Atmosukarto and Shapiro method

(2013), in that it does not create any non-salient points; all points are considered as salient, but assigned different labels. Besides, it is not established based on the classification of mid-level and low-level features of each 3D point. Instead, it uses three successive median heights of point clouds as criteria for salient point identification. In other words, the first calculated median height (z) separates all 3D points into two portions (top and bottom). Afterwards, the median height of 3D points located in the top part is used as another divider, and the median height of 3D points located in the bottom portion is applied as the third divider. By utilizing this methodology, all 3D points on each tree are divided into four groups with the equal number of points, group 1, 2, 3 and 4 from top to bottom as shown in Figure 4-2. Then, all 3D points falling into group 1 and 4 are assigned rank1, which specifies the highest and lowest part of the tree. Points in group 2 and 3 are assigned rank2, which stipulates the middle part of the tree as shown in Figure 4-3. The notes that the points should be on or inside the tree crown, so points captured out of the tree canopy, including on the ground or some objects such as cars or rocks, need to be eliminated before any calculation.

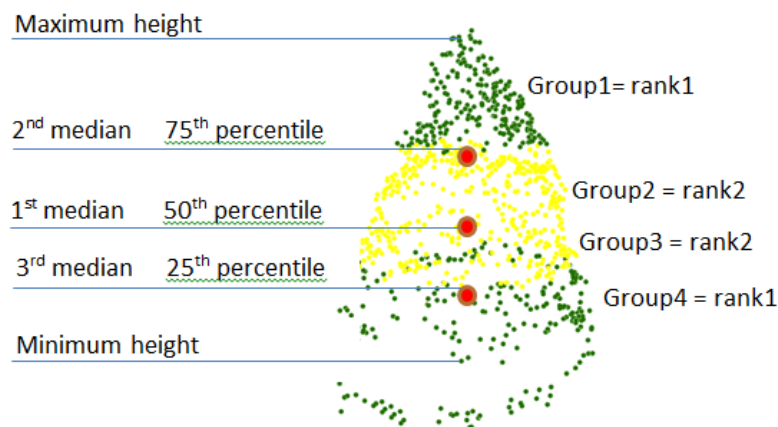


Figure 4-2 Three successive medians divide 3D point clouds into four portions

X	Y	Z	rank	XShifted	YShifted	ZShifted
513529.64	5431722.87	108	1	-1.14	-3.26	-4.59
513529.37	5431723.04	109.64	1	-1.41	-3.09	-2.95
513529.77	5431723.03	109.74	1	-1.01	-3.1	-2.85
513530.12	5431723.03	109.7	1	-0.66	-3.1	-2.89
513530.52	5431723.02	109.86	1	-0.26	-3.11	-2.73
513530.41	5431723.17	107.94	1	-0.37	-2.96	-4.65
513530.77	5431723.17	107.9	1	-0.01	-2.96	-4.69
513531.13	5431723.17	107.87	1	0.35	-2.96	-4.72
513531.49	5431723.17	107.83	1	0.71	-2.96	-4.76
513532.75	5431724.03	107.97	1	1.97	-2.1	-4.62
513532.4	5431724.03	108.02	1	1.62	-2.1	-4.57
513532.41	5431723.91	109.5	1	1.63	-2.22	-3.09
513532.15	5431723.87	109.97	1	1.37	-2.26	-2.62
513531.97	5431723.81	110.71	1	1.19	-2.32	-1.88
513531.71	5431723.79	111.08	2	0.93	-2.34	-1.51
513531.43	5431723.76	111.42	2	0.65	-2.37	-1.17
513531.08	5431723.76	111.5	2	0.3	-2.37	-1.09
513530.67	5431723.78	111.31	2	-0.11	-2.35	-1.28

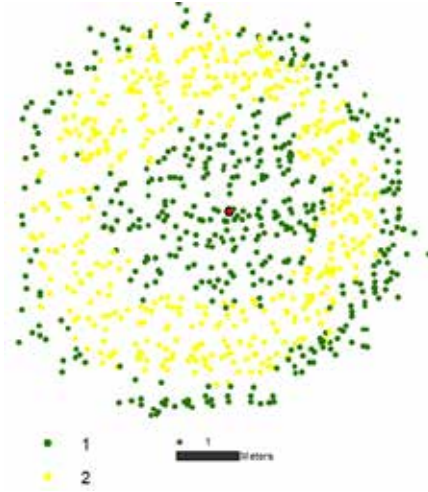


Figure 4-3. Points with rank1 are in green color, and points in rank2 are in yellow color

4.3 Simulation of LiDAR Point Clouds for the Geometrical Trees

As mentioned in 3D Shape Descriptors (3D SDs), in order to reveal the shape of trees through 3D points on or near a tree canopy, we need to have objects with a known geometrical shape for comparison. So, computer simulations were carried out using two simple geometric models, a hemisphere and a half-ellipsoid. These two models are selected, because the subjective evaluation (which is discussed in Image Similarity Assessment Techniques), suggests that the shapes of almost all evaluated trees are similar to such geometric shapes. For any random point (x, y) on a 2D Euclidean space, the z value of the point near the surface of two geometric models including a half-ellipsoid and a hemisphere can be calculated using Equation 4-1 and Equation 4-2, respectively (Dong, 2009).

$$z = f(x, y) = \sqrt{r^2 - 9 \times (x^2 + y^2)} + h \times (t - 0.5) \quad \text{Equation 4-1}$$

$$(x^2 + y^2) \leq \frac{r^2}{9}, \quad 0 \leq t \leq 1, \quad 0 \leq h \leq 1$$

$$z = f(x, y) = \sqrt{r^2 - (x^2 + y^2)} + h \times (t - 0.5) \quad \text{Equation 4-2}$$

$$(x^2 + y^2) \leq r^2, \quad 0 \leq t \leq 1, \quad 0 \leq h \leq 1$$

where, h is the amplitude of fluctuation, and t is a random number. Therefore, $h \times (t - 0.5)$ is used to add random fluctuations to the z values. So, simulated points are generated, on or

near the intended surface by using mentioned equations.

Furthermore, Dong (2010) demonstrated that LiDAR points for individual tree crowns were distributed in a layer near the crown surface. He also declared that the layer seems to be confined between a simple geometric model (such as a half-ellipsoid) and a reduced-sized model of the same shape in many cases. Therefore, for further experiments and to reflect the characteristics of the real tree, appropriate equations involved to generate points between such geometrical models.

The third dimension (z) represents the height of each LiDAR point, which is located between two surfaces of the crown, including outer surface and inner surface, so the height of any point will be randomly generated between the two surfaces $f_1(x, y)$ and $f_2(x, y)$ based on Equation 4-3 and Equation 4-4:

$$z(x, y) = f_2(x, y) \times t \quad (r^2 \leq x^2 + y^2 \leq R^2) \quad \text{Equation 4-3}$$

$$z(x, y) = f_1(x, y) + (f_2(x, y) - f_1(x, y)) \times t \quad (x^2 + y^2 < r^2) \quad \text{Equation 4-4}$$

where

$f_1(x, y)$ = The inner surface

$f_2(x, y)$ = The outer surface

Equation 4-3 and Equation 4-4 generate interior 3D points colored in red and blue in Figure 4-4, respectively.

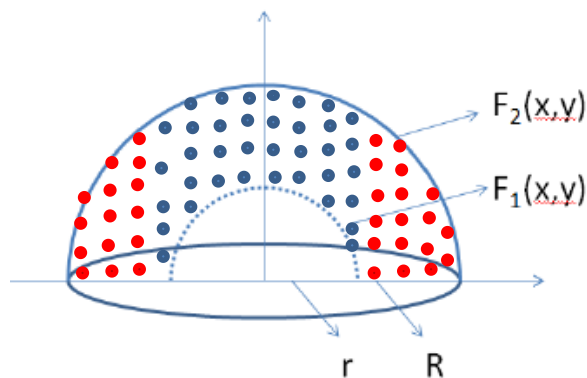


Figure 4-4. Interior 3D points generated between two surfaces of the hemisphere

For a hemisphere, $f_1(x, y)$ and $f_2(x, y)$ are determined by plugging r and R in Equation 4-2 ; the z value is demonstrated in Figure 4-5.

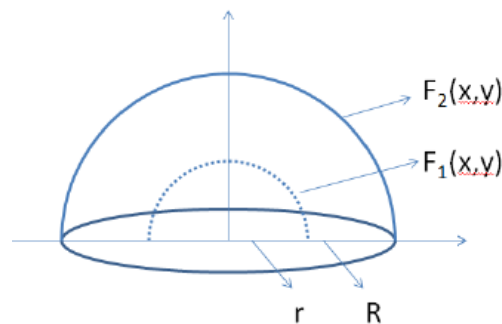


Figure 4-5. Hemisphere crown profile

For a half-ellipsoid, $f_1(x, y)$ and $f_2(x, y)$ are determined by plugging r and R in Equation 4-1; the z value is demonstrated in Figure 4-6.

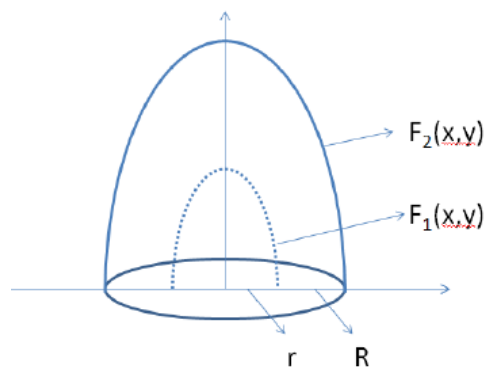


Figure 4-6. Half-ellipsoid crown profile

where

R = The outer radius of the crown

r = The inner radius of the crown

Based on the mentioned conditions, simulated 3D interior LiDAR point clouds with respective coordinates (x, y, z) in a Cartesian coordinate system are generated for two geometrical-shaped tree crowns, including the hemisphere and the half-ellipsoid using VBA programming, as shown in Figure 4-7.

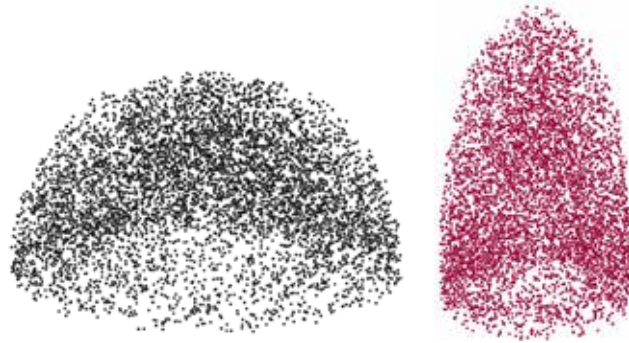


Figure 4-7. Interior 3D simulated LiDAR points for the hemisphere and the half-ellipsoid

In this study, 0.5 and 1 are assigned to r and R , respectively, and 1500 and 5000 interior 3D random points are generated based on Equation 4-3 and Equation 4-4, respectively, to have a uniform density of points.

Therefore, these simulated 3D LiDAR points of hemisphere and half-ellipsoid trees are used as objects with known geometrical shapes for further comparison aimed at identifying the shape of the examined tree based on the similarity assessment of their numerical values.

4.4 Selection of 3D LiDAR Point Clouds for Actual Trees

In this step, several real LiDAR data points for deciduous and evergreen trees are selected. Apparently, LiDAR points of deciduous trees include interior points and surface points, due to penetration of the laser beam, while LiDAR points of evergreen trees are mostly collected from their surface. In statistical analysis, at least 30 samples are required to be 95% confident, those samples would demonstrate population (Confidence intervals and sample size, 2003). Therefore, 43 trees, including 20 deciduous and 23 evergreen trees with different geometric shapes, are selected. Figure 4-8 shows distributions of all 43 selected trees, and Table 4-2 provides the position and some geometrical properties of each tree, such as width, height, and number of LiDAR points collected on each tree.

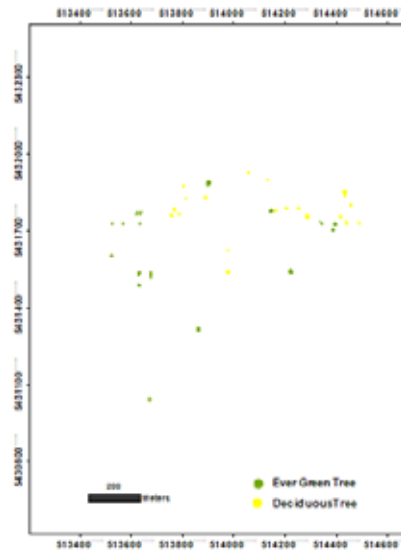


Figure 4-8. Distribution of all 43 selected trees

Table 4-2. The position and some geometrical properties of all 43 selected trees

Tree Name	Position	No of points	Width (m)	Height	Ground Height
Evergreen01	513530-5431726	927	6	9.08	107
Evergreen02	513570-5431726	734	6	9.35	108.6
Evergreen03	513634-5431532	1214	6.5	9.35	105.5
Evergreen04	513680-5431532	1089	6.2	9.6	106.4
Evergreen05	513680-5431523	1239	6.5	10.06	106
Evergreen06	513680-5431515	1317	6.6	10.75	105.8
Evergreen07	513635-5431523	784	5.8	9.36	105.6
Evergreen08	513528-5431600	1263	7.2	9.03	110.2
Evergreen09	513637-5431726	702	5.6	7.15	109.2
Evergreen10	513642-5431766	674	5.6	8.21	111.5
Evergreen11	513637-5431764	601	5.2	8.62	111.7
Evergreen12	513630-5431766	641	5.2	9.15	111.5
Evergreen13	513624-5431764	720	5.8	9.53	111.7
Evergreen14	514150-5431773	3438	10.3	19.75	114.1
Evergreen15	514400-5431724	2229	9.9	14.45	112.2
Evergreen16	514391-5431701	2004	8.3	14.94	112.1
Evergreen17	514342-5431728	605	4	2.7	111.9
Evergreen18	514349-5431725	518	3.3	3.48	111.5
Evergreen19	514227-5431536	5892	13	18.15	110.2

(table continues)

Tree Name	Position	No of points	Width (m)	Height	Ground Height
Evergreen20	513904-5431883	4854	15.4	17.4	115.8
Evergreen21	513675-5431035	1779	10.1	15.21	99.0
Evergreen22	513634-5431482	1132	7.7	10	104.8
Evergreen23	513866-5431311	2858	12.6	21.21	106.3
Deciduous01	514290-5431751	12367	14.2	17.3	113.0
Deciduous02	513792-5431763	5231	10	7.91	111.5
Deciduous03	513772-5431780	4660	8.6	8.77	110
Deciduous04	513895-5431825	2822	10.3	10.91	113
Deciduous05	513816-5431822	409	4	4.63	110
Deciduous06	513808-5431871	381	4	2.81	111
Deciduous07	513760-5431755	4994	9.8	12.59	111.6
Deciduous08	513982-5431536	4751	10.7	7.61	107.6
Deciduous09	513983-5431618	516	4.5	4.81	107.6
Deciduous10	514136-5431893	1680	6.7	7.14	112.7
Deciduous11	514061-5431922	1292	5.9	6.67	113.4
Deciduous12	514210-5431785	3556	10.2	11.6	114.07
Deciduous13	514167-5431776	1400	6.8	8.23	114.5
Deciduous14	514257-5431785	3985	10.3	10.69	114.4
Deciduous15	514438-5431848	4959	10.8	13.19	115.5
Deciduous16	514438-5431837	3882	9.9	12.4	115.3
Deciduous17	514462-5431797	2383	8.3	8.09	114.6
Deciduous18	514493-5431727	1395	6.4	12.28	115.1
Deciduous19	514443-5431728	3191	9.9	9.46	114.1
Deciduous20	514423-5431751	4132	10.3	12.33	114.4

4.5 Generation of Reference Shape Signatures from Simulated LiDAR Point Clouds

Shape signatures of the simulated trees with specific geometric models are the basis of identifying the shape of real trees, which are extracted from LiDAR point clouds. Therefore, generating their shape signatures is critical; and these shape signatures are recognized as reference shape signatures, which are considered the basis for further comparison. To

produce shape signature, first, we need to recognize salient points for each simulated tree. The proposed methodology for salient point recognition is applied on simulated 3D LiDAR points to identify interesting points, and assign rank1 and rank2 with green and yellow color. Figure 4-9 shows salient points and their corresponding ranks and colors for two hemispherical and half-ellipsoidal simulated trees.

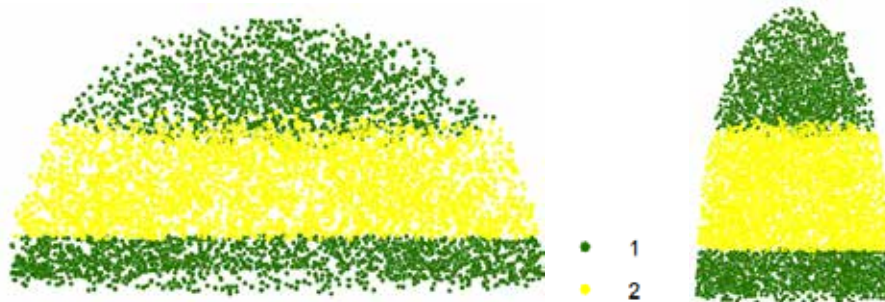


Figure 4-9. Salient points and their corresponding ranks and colors for the hemispherical and the half-ellipsoidal simulated trees

Before the generation of any shape signature, 3D points near the ground or other objects beneath the tree, such as a car, are eliminated, and the rest of the points are introduced to the following process. Since simulated LiDAR points of half-ellipsoidal and hemispherical trees are only related to trees, elimination of undesired points is not required in these cases. Afterward, 3D Cartesian coordinates of all 3D points are introduced to the longitude-latitude transformation equations, and then the 2D map of longitude and latitude positions is created by ranking, and as a result colors the longitude and latitude positions based on the rank of the initial 3D point. In other words, each transformed point on longitude-latitude map inherits the rank and color of its initial point. So, the signature map in point format is generated from 3D simulated LiDAR points. Then, natural neighbor interpolation is applied to the generated point signature map to convert it into raster format. This whole process is automated by developing an ARCGIS toolbox through Python programming to facilitate the generation of the shape signature map of any other examined tree (Figure 4-10).

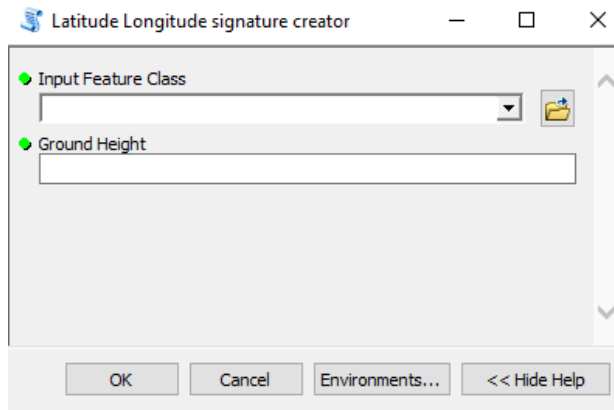


Figure 4-10. Developed ARCGIS toolbox for generation of the shape signature from point clouds

Figure 4-11 shows the pattern of salient interior points of hemispherical and half-ellipsoidal simulated trees and their corresponding map signatures in point format and raster format.

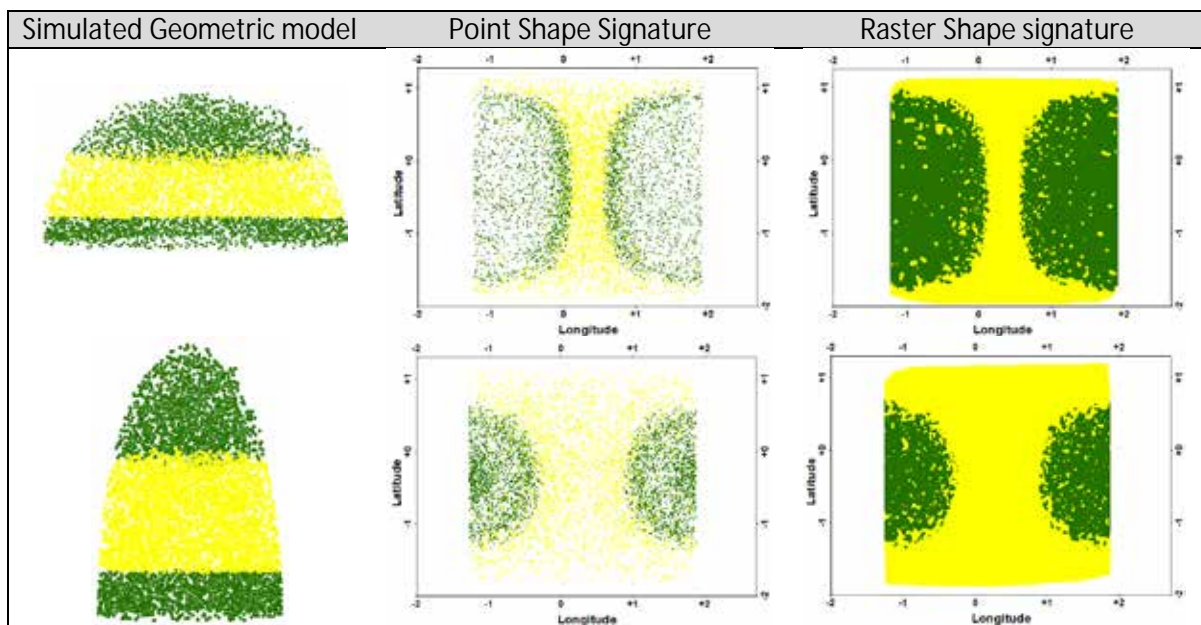


Figure 4-11. Patterns of salient interior points of hemispherical and the half-ellipsoidal simulated trees and their corresponding map signatures

Two shape signatures generated from simulated interior point clouds of the hemisphere and the half-ellipsoid demonstrate different patterns. It seems that this difference is due to the difference in their geometric shapes; in order to prove it, only surface points simulated on both geometric shapes are introduced to the toolbox for generating the

shape signatures. The shape signatures generated from interior points and surface points related to both geometric shapes, including the hemisphere and the half- ellipsoid are shown in Figure 4-12.

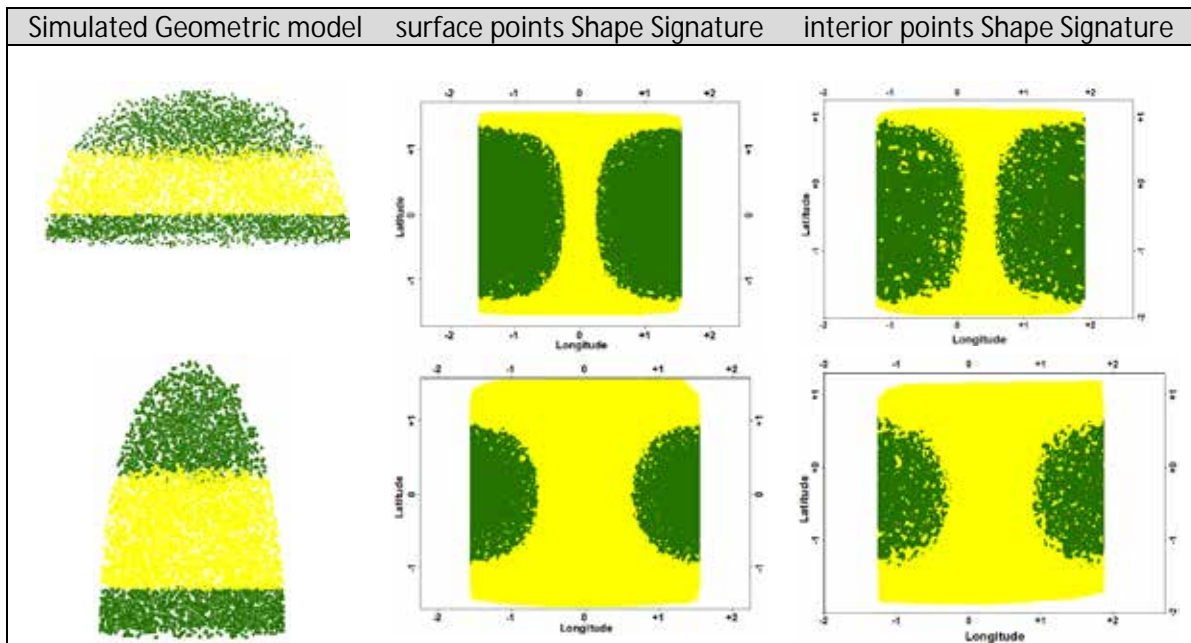


Figure 4-12. The shape signatures generated from surface points and interior points of the hemisphere and the half-ellipsoid

Visual comparison of shape signatures indicates that there is no significant difference between two shape signatures related to each geometric shape. Therefore, it can be concluded that the longitude-latitude signature map depicts the geometric shape of each model and is not sensitive to the depth of collected points. In other words, each 3D simulated tree can be separated from the other based on its corresponding 2D shape signature; no matter if their 3D points are collected from model surfaces or from inside them. Therefore, two shape signatures generated from the hemisphere and the half-ellipsoid are considered as reference shape signatures and are used as measures for discrimination of actual trees.

4.6 Generation of Evaluated Shape Signatures from Actual LiDAR Point Clouds


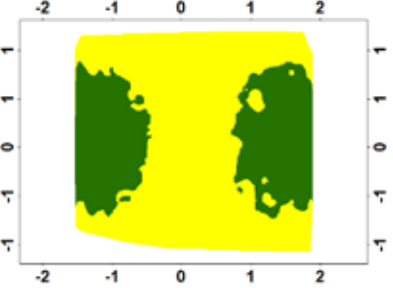



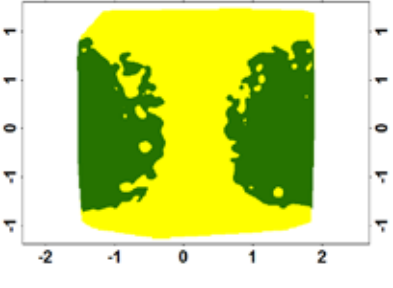

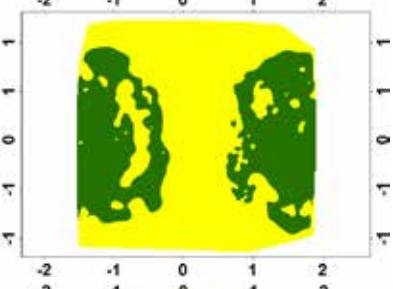

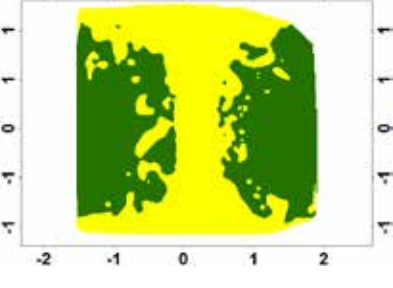
The actual LiDAR data collected from 43 trees, including deciduous and evergreen, are


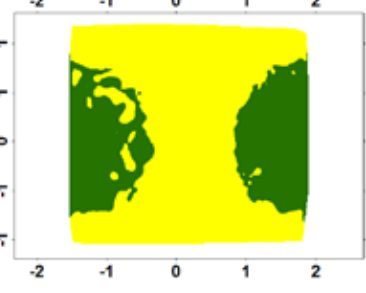

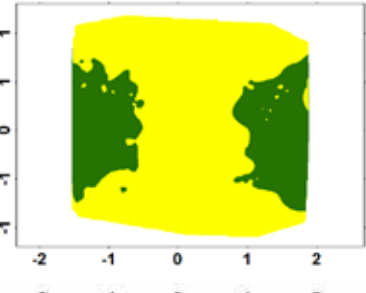

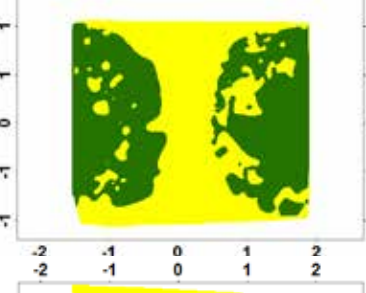

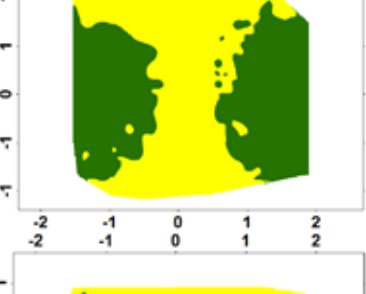

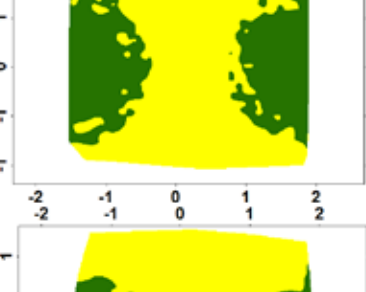

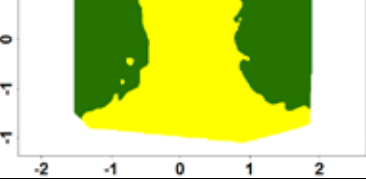
used to generate their shape signatures, which are called evaluated shape signatures or queries. The real LiDAR data include undesired points, which are mostly collected on the ground, and need to be excluded before contributing into further processing. The height of such points is extracted manually from the profile view of many points representing each tree. Then, maintained points, which represent only the tree canopy, are introduced for learning salient points; and each point is given a label, either 1 or 2. Afterward, every single point is transformed to the longitude-latitude shape signature map along with its label. Then, the natural neighbor interpolation algorithm is applied to produce the longitude-latitude shape signature in raster format. The entire mentioned process is done using the “latitude longitude signature creator” toolbox for each tree. The required times to generate longitude-latitude signature maps for trees with both the minimum and maximum number of points are presented in Table 4-3. According to Table 4-3, it takes around 13 seconds to produce the longitude-latitude shape signature map for a tree with an intermediate number of points, around 2000 points.


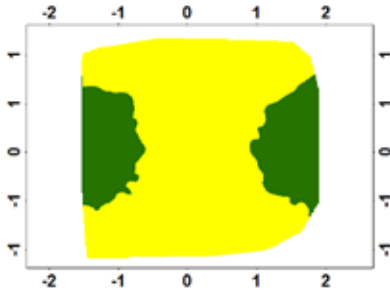

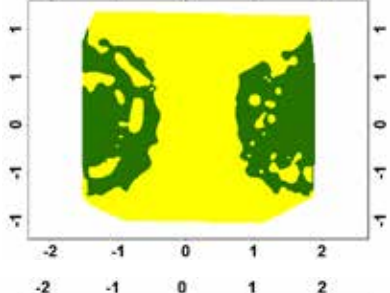

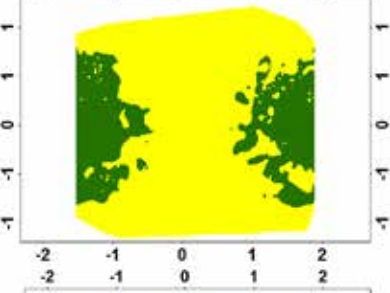

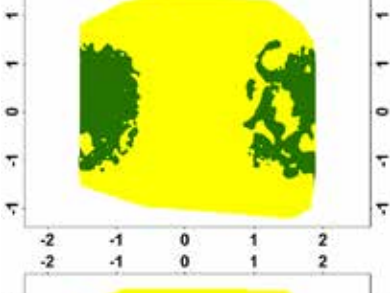

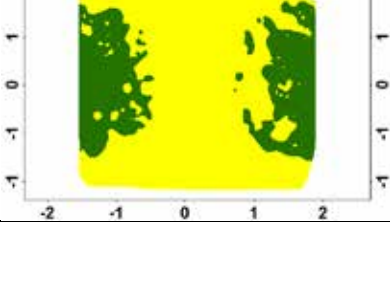
Table 4-3. Measured times to generate longitude-latitude shape signatures

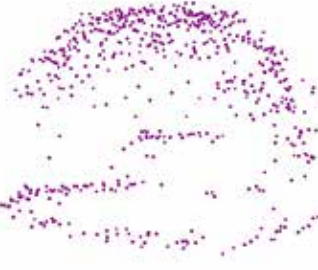
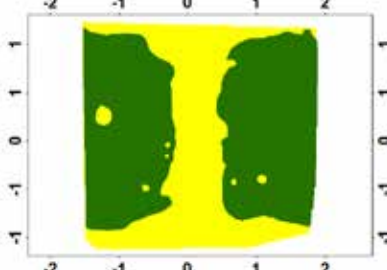

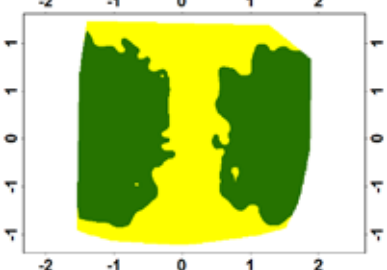

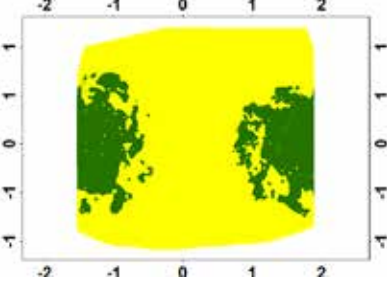

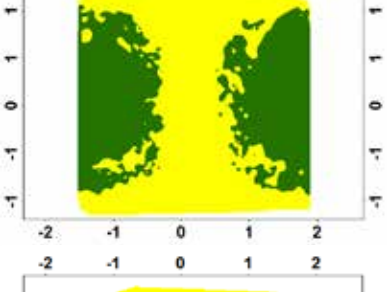

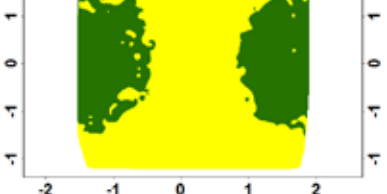
Name of tree	Number of points	Required time for shape signature generation (seconds)
Deciduous1	12367	16
Deciduous6	381	8
Half-ellipsoid and hemishere	6500	11

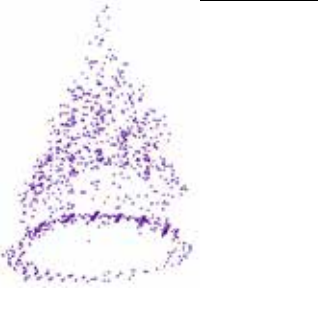
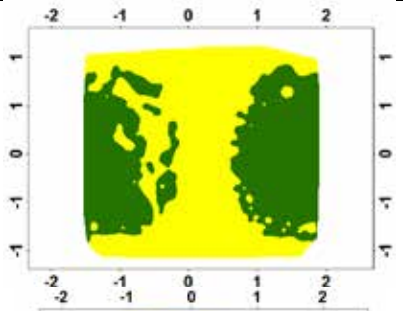

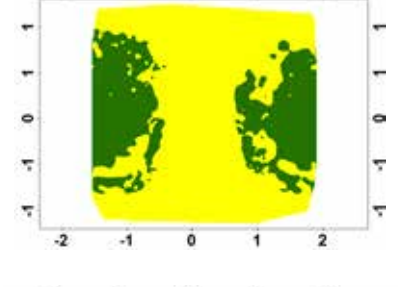

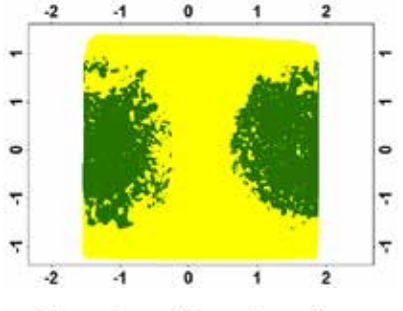

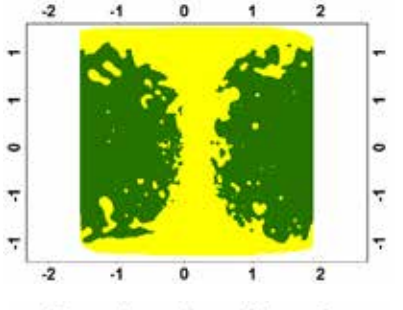
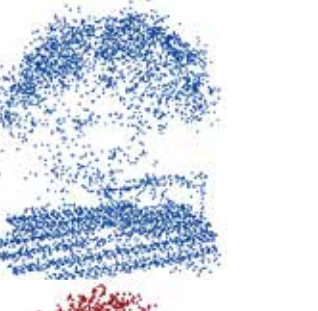
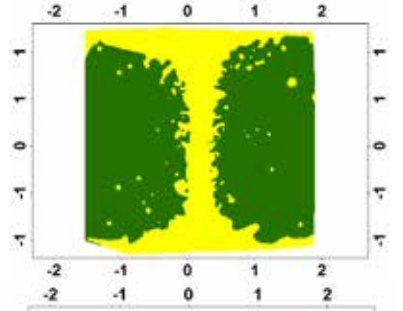

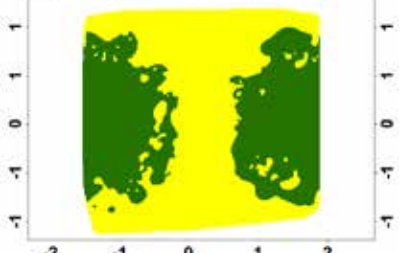
All 43 actual trees, their profile view, and their corresponding shape signature are illustrated in Figure 4-13.


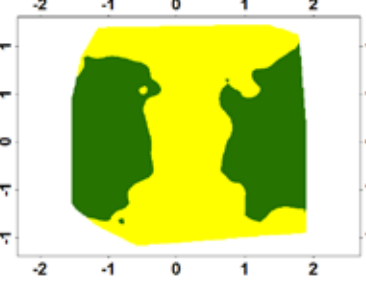
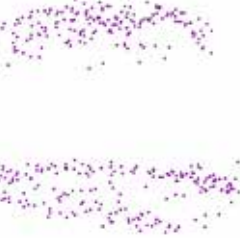
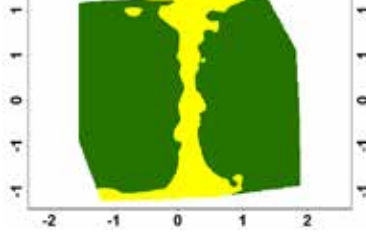

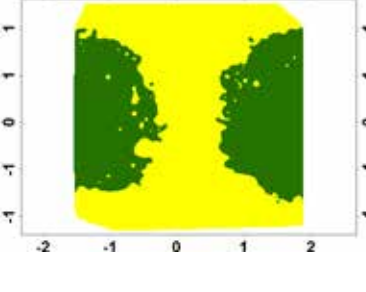

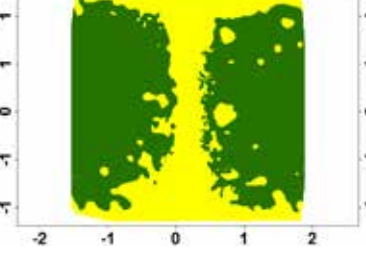
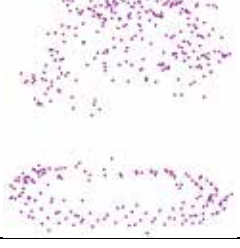
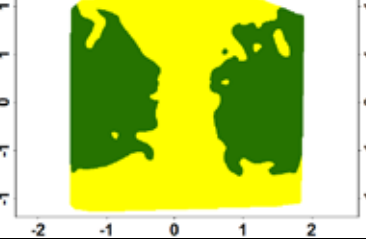
Tree Name	3D View	2D Shape Signature
Evergreen01		
Evergreen02		
Evergreen03		
Evergreen04		
Evergreen05		


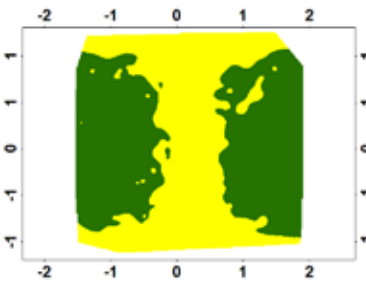

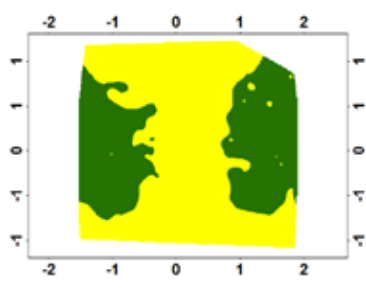

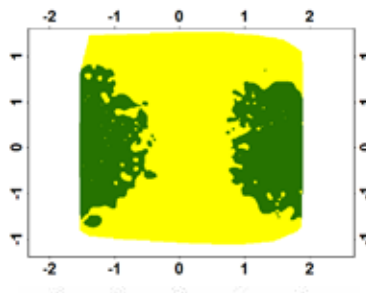
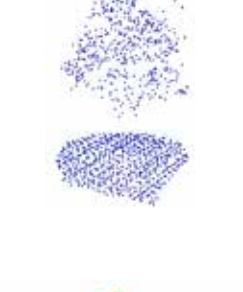
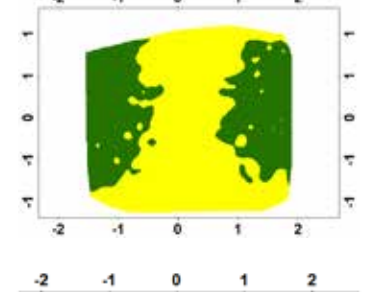

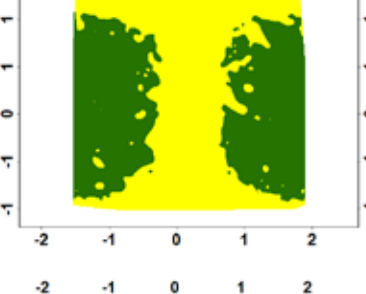

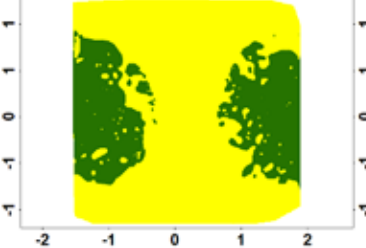
Tree Name	3D View	2D Shape Signature
Evergreen06		
Evergreen07		
Evergreen08		
Evergreen09		
Evergreen10		
Evergreen11		

Tree Name	3D View	2D Shape Signature
Evergreen12		
Evergreen13		
Evergreen14		
Evergreen15		
Evergreen16		

Tree Name	3D View	2D Shape Signature
Evergreen17		
Evergreen18		
Evergreen19		
Evergreen20		
Evergreen21		

Tree Name	3D View	2D Shape Signature
Evergreen22		
Evergreen23		
Deciduous01		
Deciduous02		
Deciduous03		
Deciduous04		

Tree Name	3D View	2D Shape Signature
Deciduous05		
Deciduous06		
Deciduous07		
Deciduous08		
Deciduous09		

Tree Name	3D View	2D Shape Signature
Deciduous10	 <p>Two views of a tree point cloud colored in cyan. The top view shows a dense, rounded canopy, and the bottom view shows a flatter, more horizontal canopy structure.</p>	 <p>A 2D heatmap showing the shape signature of the tree. The x and y axes range from -2 to 2. The plot shows two dark green regions on the left and right sides, with a yellow background in the center, indicating a symmetrical, rounded canopy.</p>
Deciduous11	 <p>Two views of a tree point cloud colored in light green. The top view shows a dense, rounded canopy, and the bottom view shows a canopy with distinct horizontal lines, suggesting a layered or structured canopy.</p>	 <p>A 2D heatmap showing the shape signature of the tree. The x and y axes range from -2 to 2. The plot shows two dark green regions on the left and right sides, with a yellow background in the center, indicating a symmetrical, rounded canopy.</p>
Deciduous12	 <p>Two views of a tree point cloud colored in brown. The top view shows a dense, rounded canopy, and the bottom view shows a canopy with a distinct horizontal line, suggesting a layered or structured canopy.</p>	 <p>A 2D heatmap showing the shape signature of the tree. The x and y axes range from -2 to 2. The plot shows two dark green regions on the left and right sides, with a yellow background in the center, indicating a symmetrical, rounded canopy.</p>
Deciduous13	 <p>Two views of a tree point cloud colored in purple. The top view shows a dense, rounded canopy, and the bottom view shows a flatter, more horizontal canopy structure.</p>	 <p>A 2D heatmap showing the shape signature of the tree. The x and y axes range from -2 to 2. The plot shows two dark green regions on the left and right sides, with a yellow background in the center, indicating a symmetrical, rounded canopy.</p>
Deciduous14	 <p>Two views of a tree point cloud colored in green. The top view shows a dense, rounded canopy, and the bottom view shows a canopy with a distinct horizontal line, suggesting a layered or structured canopy.</p>	 <p>A 2D heatmap showing the shape signature of the tree. The x and y axes range from -2 to 2. The plot shows two dark green regions on the left and right sides, with a yellow background in the center, indicating a symmetrical, rounded canopy.</p>
Deciduous15	 <p>Two views of a tree point cloud colored in teal. The top view shows a dense, rounded canopy, and the bottom view shows a canopy with a distinct horizontal line, suggesting a layered or structured canopy.</p>	 <p>A 2D heatmap showing the shape signature of the tree. The x and y axes range from -2 to 2. The plot shows two dark green regions on the left and right sides, with a yellow background in the center, indicating a symmetrical, rounded canopy.</p>

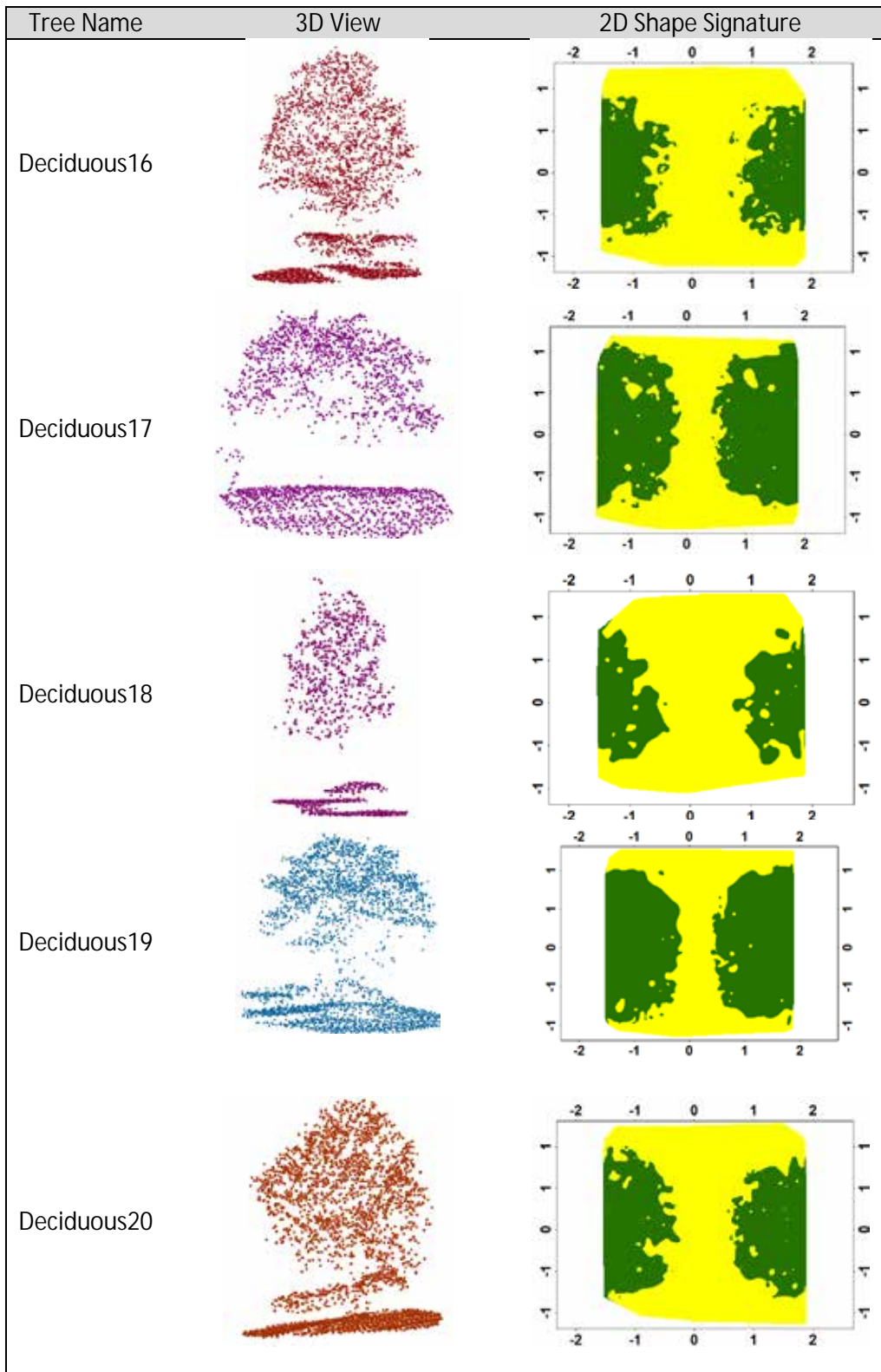


Figure 4-13. The profile view of each 43 actual trees, and their corresponding shape signatures

4.7 Similarity Assessment between Evaluated and Reference Shape Signatures

As mentioned in Image Similarity Assessment Techniques, there are two approaches

for image similarity assessment: subjective and objective measurement. Hence, 3D shape signatures generated from two simulated crowns, including the hemisphere and the half-ellipsoid, can be used as measures for similarity assessment of shape signatures produced from each of the 43 actual trees. In other words, reference shape signatures are used as criteria for similarity assessment of each evaluated shape signature.

4.7.1 Subjective Similarity Assessment

This approach involves human perceptions of similarity, in which an observer is asked to score the similarity of the evaluated shape signature and reference shape signature. So, similarity of the evaluated shape signature could be assessed by comparing it against the reference shape signature. A measure of the similarity between the reference image and the image being evaluated could be calibrated to serve as a perceptual quality measure. Visual comparison of shape signatures of the hemisphere and the half ellipsoid indicates that the green part of the hemisphere signature is more widespread than the ellipsoid signature, as displayed in Figure 4-14. This straightforward difference between these two reference shape signatures is used as a criterion for subjective assessment of signatures generated from the other 43 actual trees to identify their shapes, and as a result to discriminate all evaluated trees.

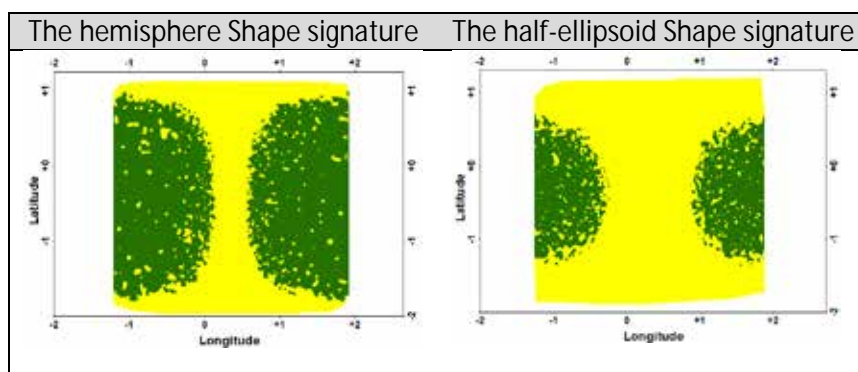


Figure 4-14. The green part of the hemisphere signature is more widespread than green part of the ellipsoid signature, which is used as a criterion for subjective similarity assessment

This approach for tree crown shape discrimination is time consuming and inconvenient, and the results might vary depending on the observer. Besides, it is an inefficient approach, especially for trees whose shape is close to both geometric models, including the hemisphere and the half-ellipsoid. All mentioned shortcomings made us use objective similarity assessment rather than the subjective approach.

4.7.2 Objective Similarity Assessment

In this study, two objective techniques, including Mean Squared Error (MSE) and Peak Signal to Noise Ratio (PSNR), are applied for similarity assessment between an evaluated shape signature and a reference shape signature. To facilitate similarity assessment by MSE technique, an ArcGIS toolbox named "Mean Squared Error" is developed, using existing models in other toolboxes, and its interface is shown in Figure 4-15. So, in order to find out the shape of each actual tree by this tool, the shape signature resulting from LiDAR points of that tree is introduced as the evaluated shape signature and the shape signature resulting from each geometric model, either the hemisphere or the half-ellipsoid, is plugged as the reference shape signature in each step. This tool runs and calculates MSE, which takes approximately 7 seconds. As mentioned in Image Similarity Assessment Techniques, the lower MSE value indicates greater similarity. Lastly, the shape of the geometric model that produces the lower MSE is assigned to the evaluated tree.

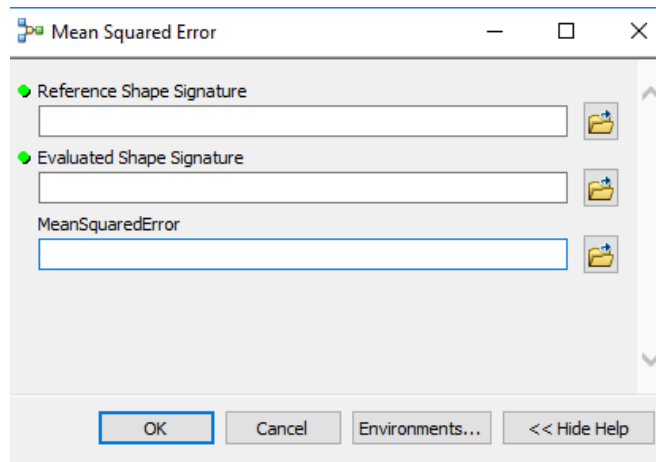


Figure 4-15. Developed ArcGIS toolbox named “Mean squared Error” for MSE similarity assessment

Afterward, Excel software is used to calculate PSNR by plugging already measured MSE corresponding to each actual tree and each geometric model. Unlike MSE with PSNR, higher values indicate greater image similarity. All calculated MSEs and PSNRs corresponding to each actual tree are listed in Table 4-4, which are used to specify the most similar geometric shape to each evaluated tree.

Therefore, two MSEs and two PSNRs are calculated for each evaluated tree for two geometric models, including the half-ellipsoid and the hemisphere. The most similar geometric model to each evaluated tree is the one with lower MSE, and as a result, higher PSNR.

Table 4-4. MSEs and PSNRs corresponding to each actual tree and each geometric model, which are used for detecting the most similar shape to each actual tree

type of tree	MSE		PSNR		Similar Geometric Shape
	Half-ellipsoid	Hemispher e	Half-ellipsoid	Hemispher e	
Evergreen1	0.07	0.22	5.77	3.29	Ellipsoid
Evergreen2	0.08	0.19	5.48	3.61	Ellipsoid
Evergreen3	0.13	0.16	4.43	3.98	Ellipsoid
Evergreen4	0.16	0.18	3.98	3.72	Ellipsoid
Evergreen5	0.2	0.1	3.49	5.00	Hemisphere
Evergreen6	0.07	0.25	5.77	3.01	Ellipsoid
Evergreen7	0.06	0.28	6.11	2.76	Ellipsoid

(table continues)

type of tree	MSE		PSNR		Similar Geometric Shape
	Half-ellipsoid	Hemisphere	Half-ellipsoid	Hemisphere	
Evergreen8	0.21	0.13	3.39	4.43	Hemisphere
Evergreen9	0.14	0.13	4.27	4.43	Hemisphere
Evergreen10	0.06	0.25	6.11	3.01	Ellipsoid
Evergreen11	0.06	0.24	6.11	3.10	Ellipsoid
Evergreen12	0.07	0.35	5.77	2.28	Ellipsoid
Evergreen13	0.1	0.24	5.00	3.10	Ellipsoid
Evergreen14	0.09	0.33	5.23	2.41	Ellipsoid
Evergreen15	0.09	0.36	5.23	2.22	Ellipsoid
Evergreen16	0.1	0.3	5.00	2.61	Ellipsoid
Evergreen17	0.32	0.06	2.47	6.11	Hemisphere
Evergreen18	0.25	0.07	3.01	5.77	Hemisphere
Evergreen19	0.1	0.35	5.00	2.28	Ellipsoid
Evergreen20	0.15	0.15	4.12	4.12	Ellipsoid & Hemisphere
Evergreen21	0.06	0.26	6.11	2.93	Ellipsoid
Evergreen22	0.16	0.15	3.98	4.12	Hemisphere
Evergreen23	0.11	0.25	4.79	3.01	Ellipsoid
Deciduous1	0.1	0.22	5.00	3.29	ellipsoid
Deciduous2	0.27	0.07	2.84	5.77	Hemisphere
Deciduous3	0.38	0.07	2.10	5.77	Hemisphere
Deciduous4	0.17	0.14	3.85	4.27	Hemisphere
Deciduous5	0.13	0.14	4.43	4.27	ellipsoid
Deciduous6	0.43	0.1	1.83	5.00	Hemisphere
Deciduous7	0.16	0.15	3.98	4.12	Hemisphere
Deciduous8	0.32	0.07	2.47	5.77	Hemisphere
Deciduous9	0.16	0.12	3.98	4.60	Hemisphere
Deciduous10	0.21	0.09	3.39	5.23	Hemisphere
Deciduous11	0.11	0.18	4.79	3.72	ellipsoid
Deciduous12	0.07	0.24	5.77	3.10	ellipsoid
Deciduous13	0.1	0.19	5.00	3.61	ellipsoid
Deciduous14	0.19	0.12	3.61	4.60	Hemisphere
Deciduous15	0.09	0.25	5.23	3.01	ellipsoid
Deciduous16	0.09	0.22	5.23	3.29	ellipsoid
Deciduous17	0.26	0.07	2.93	5.77	Hemisphere
Deciduous18	0.07	0.28	5.77	2.76	ellipsoid
Deciduous19	0.28	0.06	2.76	6.11	Hemisphere
Deciduous20	0.13	0.17	4.43	3.85	ellipsoid

According to the results shown in Table 4-4, it can be inferred that regardless of the leaf trait of each actual tree, including deciduous and evergreen, the tree canopy shape, either hemisphere or half-ellipsoid, can be identified with the longitude-latitude shape signature in

any case as listed in Table 4-5.

Table 4-5. Tree canopy can be hemisphere or half-ellipsoid regardless of its leaf trait, which can be identified by its corresponding longitude-latitude shape signature

	type of tree
Ellipsoid	Evergreen1
	Evergreen2
	Evergreen3
	Evergreen4
	Evergreen6
	Evergreen7
	Evergreen10
	Evergreen11
	Evergreen12
	Evergreen13
	Evergreen14
	Evergreen15
	Evergreen16
	Evergreen19
	Evergreen21
	Evergreen23
	Deciduous1
	Deciduous5
	Deciduous11
	Deciduous12
Deciduous13	
Deciduous15	
Deciduous16	
Deciduous18	
Deciduous20	
Ellipsoid & Hemisphere	Evergreen20
Hemisphere	Evergreen5
	Evergreen8
	Evergreen9
	Evergreen17
	Evergreen18
	Evergreen22
	Deciduous2
	Deciduous3
	Deciduous4
	Deciduous6
	Deciduous7
	Deciduous8
	Deciduous9
	Deciduous10
Deciduous14	
Deciduous17	
Deciduous19	

In other words, leaf trait of the evaluated tree has no severe impact on its longitude-latitude signature map. The mathematical reason is explained as follows: Given the surface normal vector $n(n_x, n_y, n_z)$ of a 3D point P , the azimuth angle θ of n is defined as the angle between the positive xz plane and the projection of n to the x plane. The elevation angle φ of n is defined as the angle between the x plane and vector n (Atmosukarto & Shapiro, 2013). Figure 4-16 illustrates the graphical view of the longitude and the latitude of a 3D point P .

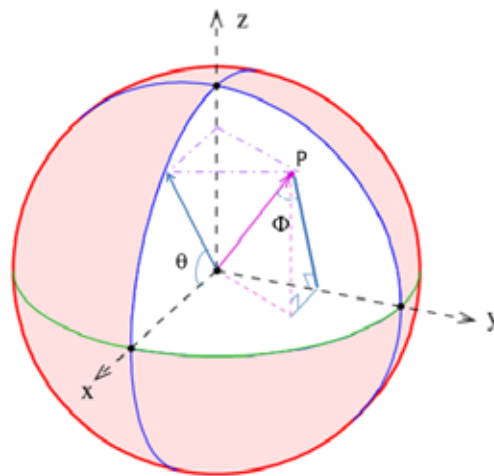


Figure 4-16. θ and φ of a single 3D point P

If two points P and P' are aligned with the local origin, then their normal vector n , and as a result, their longitude and latitude are the same, as illustrated in Figure 4-17.

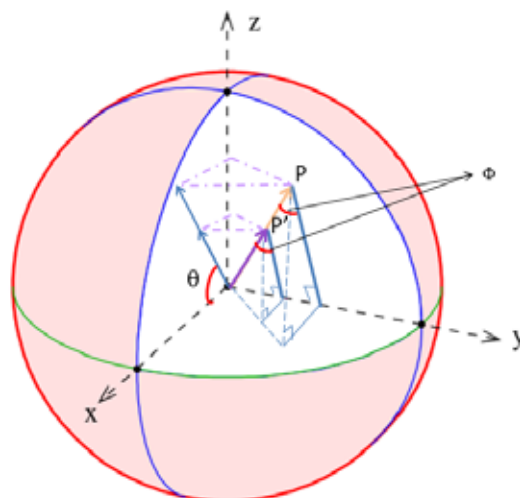


Figure 4-17. Two points P and P' aligned with the local origin have the same normal vector n , and the same longitude and latitude

So, it can be concluded that interior points, collected inside a tree by LiDAR, do not have severe effects on its corresponding shape signature. Therefore a longitude-latitude shape signature is a function of the tree's geometric shape, regardless of the depth of LiDAR points collected by LiDAR.

Even though similarity assessment can be done by subjective and objective approaches, subjective approaches are not recommended because it is impossible to implement it into an automatic real-time system (Varnan, Jagan, Kaur, Jyoti, & Rao, September 2011). Objective evaluations are automatic, and defined by mathematical algorithms; however, subjective measurements should be used to validate the accuracy of objective measures. In this study, subjective similarity assessment, in either the real-world domain or shape signature domain, approves objective similarity assessment results in most cases such as evergreen1 and deciduous3, as shown in Figure 4-18 and Figure 4-19, respectively. While, in some cases, such as evergreen9 shown in Figure 4-20, the visual comparison is not able to identify the exact shape of the tree canopy, we can rely on the objective similarity assessment result.



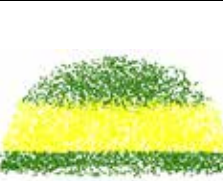
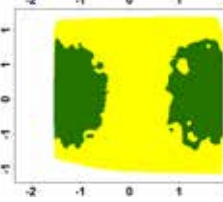
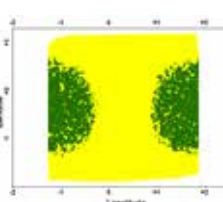
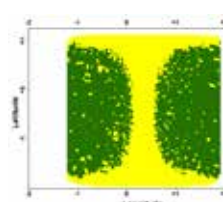
	Evergreen1	Half-ellipsoid	Hemisphere	Similarity assessment	
				subjective	Objective
actual shape domain					
shape signature domain				Half-ellipsoid	Half-ellipsoid

Figure 4-18. Visual comparison of shape signatures or 3D profile views approve objective similarity assessment result for evergreen1




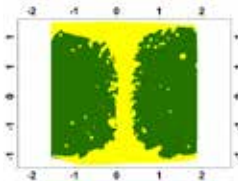
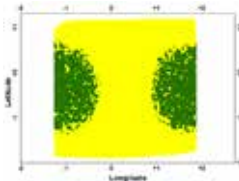
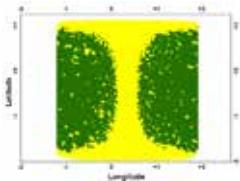
		Deciduous3	Half-ellipsoid	Hemisphere	Similarity assessment	
					subjective	Objective
actual shape domain				Hemisphere		
				Hemisphere		
shape signature domain				Hemisphere		

Figure 4-19. Visual comparison of shape signatures or 3D profile views approve objective similarity assessment result for deciduous3




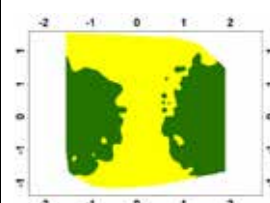
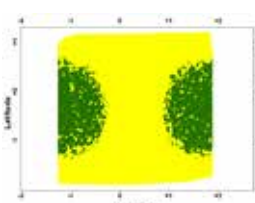
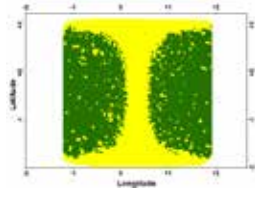
		Evergreen9	Half-ellipsoid	Hemisphere	Similarity assessment	
					subjective	Objective
actual shape domain				Not able		
				Hemisphere		
shape signature domain				Not able		

Figure 4-20. Visual comparison is not able to identify the exact shape of tree canopy for evergreen9, so that we can rely on objective similarity assessment result

CHAPTER 5

RESULTS AND DISCUSSION

To investigate the success of the latitude-longitude shape descriptor and all proposed steps in tree crown discrimination, my thesis study has been designed to determine whether the desirable properties required for an effective shape descriptor are fulfilled or not. The experimental results from the latitude-longitude shape descriptor suggest that all desirable properties are provided by this shape descriptor for tree crown discrimination as follows.

- Uniqueness: the longitude-latitude shape signature related to each tree is uniquely coupled with that unique tree.
- Discriminative accuracy: trees that are found perceptually similar in their geometric shape have similar shape signatures and are different from others. In other words, the longitude-latitude shape signature can distinguish half-ellipsoidal-shaped trees from hemispherical-shaped trees accurately.
- Well-defined range: any longitude-latitude shape signature has a range of values between -1.5 and 1.5 on both horizontal and vertical axes. Therefore, normalization is not required for analysis and comparison.
- Rotation invariance: rotation of tree does not affect its shape signature, and its longitude-latitude shape descriptor produces the same measure for a tree rotated by any degrees.
- Translation invariance: location of the tree does not affect its shape signature, and its longitude-latitude shape descriptor produces the same results regardless of the tree's location.
- Scale invariance: The scale of each tree, including width and height, does not affect the measure produced by the longitude- latitude shape descriptor.

- Insensitive to noise: longitude-latitude shape signatures are relatively insensitive to noise and other small local variations; this insensitivity is vital for canopy shape discrimination in real-world environments.

- Efficient regarding computational performance and memory: the entire process from creating a shape signature and its similarity assessment for a tree with an intermediate number of 3D points (2000 points) takes around 20 seconds using both developed ArcGIS toolboxes.

All of the above desirable properties are suggested in the computer science field, whereas in this study due to dealing with LiDAR point clouds, another desirable property is found in the longitude-latitude shape descriptor for tree crown discrimination as follows:

- Leaf-off, leaf-on invariance: the longitude-latitude shape signature is not sensitive to the presence or absence of interior points. In other words, deciduous or evergreen trees with the same exterior shape exhibit similar shape signatures. Therefore, the depth of penetration of LiDAR does not have a severe impact on the pattern of longitude-latitude shape signatures, which makes this process autonomous from the acquisition date of LiDAR data.

CHAPTER 6

CONCLUSION

The primary objective of this study is to develop a modified 3D shape descriptor for the discrimination of different tree crown shapes using LiDAR point clouds. According to the obtained experimental results, this study is finally able to answer the following research questions:

- (1) Which existing 3D shape descriptor is recommended in computer graphics for 3D object retrieval?

As mentioned in 3D Shape Descriptors (3D SDs), view-based and histogram-based algorithms are the most favored SDs, because of their fundamental decency and performance (Khalid Kazmi, You, & Zhang, 2013). So, to benefit from the advantages of histogram-based SDs, in this study a histogram-based SD called longitude-latitude SD is used, which falls explicitly into the shape spectrum subcategory.

Atmosukarto and Shapiro (2008), in the field of computer science, examined the efficiency of a longitude-latitude transformation as a shape-based descriptor to retrieve 3D objects. They contributed longitude-latitude shape signatures of different heads of various objects for 3D object retrieval purpose. Finally, according to their experimental results, Atmosukarto and Shapiro (2008) concluded that the 2D longitude-latitude map signature achieved a good retrieval score for 3D object recognition. This study motivated me to inquire performance and repeatability of the longitude-latitude shape descriptor for discrimination of individual tree crowns derived from Light Detection and Ranging (LiDAR).

- (2) How should a successful 3D shape descriptor in computer graphics modify for effective tree crown shape discrimination applied on LiDAR data?

To achieve that goal, this study proposed a methodology which comprises of five main components, including a definition of a local coordinate system, learning salient points,

generation of simulated LiDAR point clouds with geometrical shape, shape signature generation from simulated LiDAR points and actual LiDAR point clouds, and finally similarity assessment of shape signatures.

In the first component, a new origin is defined inside each tree by calculating the median value of the x , y and z positions of all 3D points on each tree, either simulated or actual point clouds. Then the x , y , z coordinates of 3D point clouds are transformed to this new origin.

In the second component, a new methodology is proposed for learning salient points, which differs from Atmosukarto and Shapiro method (2013). It uses three successive median heights of point clouds as criteria for salient point identification.

In the third component, two geometric trees, including a half-ellipsoid and a hemisphere, were simulated and contributed as measures for differentiation of actual tree crowns. This approach differs from the Atmosukarto and Shapiro method (2013) in that it does not use any real tree data as a measure, which needs field data collection.

In the fourth component, all points related to each tree, either simulated or actual trees, are converted to their longitude-latitude positions, and then a signature map in point format is generated for every tree. Afterward, natural neighbor interpolation is applied on the longitude-latitude signature map in point format to produce the longitude-latitude signature map in raster format. This component also differs from Atmosukarto and Shapiro method (2013) in that rasterization is applied after signature map generation, instead of surface mesh creation from digitized 3D objects at the initial step. Additionally, it differs from Dong method (2010) in that it generates a 2D raster signature map, instead of the curved-shaped signature map.

(3) Can simulated LiDAR point clouds for geometrical-shaped trees be used as references to reveal the shape of real LiDAR point clouds of actual trees?

3D LiDAR points on 43 actual trees in the city of Surrey, British Columbia (Canada) with both leaf traits, including deciduous and evergreen are examined, and their shape signatures are generated, which are called evaluated shape signatures. The longitude-latitude signatures produced from half-ellipsoidal and hemispherical trees are used as measures for tree crown discrimination and called reference shape signatures. Finally, for similarity assessment as the last component, two widely used objective approaches, including MSE and PSNR were applied, which compare two raster maps and evaluate their similarity. The most similar geometric shape to each actual tree is the one having lower MSE and higher PSNR.

(4) How can we automatically discriminate three-dimensional tree crown shapes using LiDAR data?

The entire process of creating a shape signature and its similarity assessment is implemented automatically by two developed ArcGIS toolboxes and takes around 20 seconds for each tree.

Experimental results indicate that subjective similarity assessment in all 43 cases approves the objective similarity assessment, which means that the comparison of 3D canopy shapes of trees can be effectively reduced to the comparison of 2D longitude-latitude signatures. The obtained results also indicate that the longitude-latitude shape descriptor fulfills all desired properties of a good shape signature, such as uniqueness, discriminative accuracy, well-defined range, rotation invariance, translation invariance, scale invariance and insensitivity to noise. Besides, leaf trait of the evaluated tree does not affect its shape signature, which means that the longitude-latitude signature is Leaf-off, leaf-on invariance. In other words, deciduous or evergreen trees with the same exterior shape exhibit similar shape signatures, which make this process autonomous from the acquisition date of LiDAR data.

In summary, we can automatically discriminate tree crowns of various trees using their corresponding longitude-latitude shape signatures derived from LiDAR point clouds acquired in any date.

REFERENCES

- Airborne Imaging. (2013). *Final report for project: city of Surrey*. Calgary.
- Atmosukarto, I., & Shapiro, L. (2008). A Salient-Point Signature for 3D Object Retrieval. *The 1st ACM international conference on Multimedia information retrieval*.
- Atmosukarto, I., & Shapiro, L. (2013). 3D object retrieval using salient views. *Int J Multimed Inf Retr*, 103–115.
- Confidence intervals and sample size*. (2003). Retrieved from file:///C:/Users/Fariba/Downloads/ch07.pdf
- Dong, P. (2009). Characterization of individual tree crowns using three-dimensional shape signatures derived from LiDAR data. *International Journal of Remote Sensing*, 6621–6628.
- Dong, P. (2010). Sensitivity of LiDAR-derived three-dimensional shape signatures for individual tree crowns: a simulation study. *Remote Sensing Letters*, 159-167.
- Ghosha, A., Fassnacht, F., Joshi, J., & Koch, B. (2014). *A framework for mapping tree species combining hyperspectral and LiDAR data: Role of selected classifiers and sensor across three spatial scales*. International Journal of Applied Earth Observation and Geoinformation.
- Iyer, N., Jayanti, S., Lou, K., Kalyanaraman, Y., & Ramani, K. (2005). Three-dimensional shape searching: state-of-the-art. *Computer-Aided Design*, vol. 37, no.5, 509–530.
- Jakubowski, M., Li, W., Guo, Q., & Kelly, M. (2013). *delineating individual trees from LiDAR data: a comparison of vector-based and raster-based segmentation approaches*. remote sensing journal.
- Kato, A., Moskal, L., Schiess, P., Swanson, M., Calhoun, D., & Stuetzle, W. (2009). *Capturing tree crown formation through implicit surface reconstruction using airborne lidar data*. Remote Sensing of Environment.
- Khalid Kazmi, I., You, L., & Zhang, J. (2013). A Survey of 2D and 3D Shape Descriptors. *10th International Conference Computer Graphics, Imaging and Visualization*, (pp. 1-10).
- Lichstein, J. (2010). unlocking the forest inventory data: relating individual tree performance to unmeasured environmental factors. *Ecological Applications* 20 (3), 684-699.
- Liu, H. (2013). *Automated Treetop Detection and Tree Crown Identification Using Discrete-return LiDAR Data*. Denton: University of North Texas.
- Martinez-Ortiz, C. (2010). *2D and 3D shape descriptors*. Department of computer science, university of Exeter.

- Omasa, K., & Fumiki, H. (2007). Factors contributing to accuracy in the estimation of the woody canopy leaf area density profile using 3D portable lidar imaging. *Journal of Experimental Botany* 58.12, 3463-3473.
- Osada, R., Funkhouser, T., Chazelle, B., & Dobkin, D. (2002). Shape distribution. *ACM Transactions on Graphics*, 21, 807–832.
- Plowright, A., Coops, N., Eskelson, B., Sheppard, S., & Aven, N. (2016). Assessing urban tree condition using airborne light detection and ranging. *Urban Forestry & Urban Greening*, 140–150.
- Sexon, A., Bax, T., Siqueira, P., Swenson, J., & Hensley, S. (2009). A comparison of LiDAR, radar, and field measurements of canopy height in pine and hardwood forests of southeastern North America. *Forest ecology and management* 257, 1136-1147.
- Varnan, C., Jagan, A., Kaur, J., Jyoti, D., & Rao, D. (September 2011). Image quality assessment techniques on spatial domain. *International Journal of Computer Science and Technology*, Vol. 2, Issue 3, 177-184.
- Xiao, W. (2012). *detection changes in trees using multi-temporal airborne lidar point clouds*. Netherland: faculty of geo-information science and earth observation of the university of Twente.
- Yang, M., Kpalma, K., & Ronsin, J. (2008). A survey of shape feature extraction techniques. *Pattern Recognition*.
- Zaharia, T., & Preteux, F. (January 2001). Three-dimensional shape-based retrieval within the MPEG-7 framework. *SPIE Conference on Nonlinear Image Processing and Pattern Analysis XII* (pp. 133-145). San Jose, CA: Vol. 4304.